STRESSES IN HEAVY SECTION ELECTROSLAG JOINING

by

PAULO SILVEIRA IVO

B.A.Sc.,Universidade Federal de Minas Gerais, Brasil,1978

A THESIS SUBMITTED IN PARTIAL FULFILMENT OF

THE REQUIREMENTS FOR THE DEGREE OF

MASTER OF APPLIED SCIENCE

in

THE FACULTY OF GRADUATE STUDIES

Department of Metallurgical Engineering

We accept this thesis as conforming

to the required standard

THE UNIVERSITY OF BRITISH COLUMBIA

October 1982

In presenting this thesis in partial fulfilment of the requirements for an advanced degree at the University of British Columbia, I agree that the Library shall make it freely available for reference and study. I further agree that permission for extensive copying of this thesis for scholarly purposes may be granted by the Head of my Department or by his or her representatives. It is understood that copying or publication of this thesis for financial gain shall not be allowed without my written permission.

Department of Metallurgical Engineering

The University of British Columbia
2075 Wesbrook Place
Vancouver, Canada
V6T 1W5

Date: October 05, 1982

Abstract

A study of the thermal stresses resulting in the Electroslag Joining Process as applied to heavy gauge forgings has been undertaken, since a survey of published reports on the process indicates that although solidification cracking ought to be a problem, apparently it is not routinely observed. Welding conditions which are known to produce solidification cracks in Electroslag Welding with wire electrodes were reported to make crack-free welds using ESJ plate electrodes.

This study reports work on the thermal and stress fields developed during ESJ of 150 mm thick A36 steel plates. Conditions predicted by previous workers to form cracks with wire electrodes were established and found not to form cracks with plate electrodes. Measurements of stress and temperature during welding were made and found to agree well with a simple numerical model of the process.

It is concluded that the thermal field of ESJ is sufficiently different to ESW that it can relax the stress field developed, even in a fully-constrained joint, to the point at which solidification cracking is no longer observed.

Table of Contents

Abstract ii
List of Tables v
List of Figures vi
Acknowledgement viii
I. INTRODUCTION 1
1.1 Introduction 1
1.2 Process Description and Application 3
1.3 Previous Work 6
1.4 Solidification Cracking 9
1.5 Present Objectives 12
II. MATHEMATICAL MODELING 13
2.1 Temperature Distribution Calculation 14
2.1.1 Assumptions 14
2.1.2 Derivation Of Equations 16
2.1.3 Numerical Solution 17
2.2 Thermal Stress And Strain Calculation 18
2.3 Computer Production Runs 21
III. EXPERIMENTAL WORK 23
3.1 Furnace Design 23
3.2 Cooling Shoe Design 23
3.3 Electrode And Slag Preparation 24
3.4 Weld Set-up And Constraining 26
3.5 Sequence of Operation - Welding Procedure 28
3.6 Residual Stress 29

3.7 Temperature Measurements 29

IV. DISCUSSION AND RESULTS 31

V. CONCLUSIONS 35

VI. SUGGESTIONS FOR FUTURE WORK 36

BIBLIOGRAPHY 37

APPENDIX A - BOUNDARY CONDITIONS 68

APPENDIX B - COMPUTER PROGRAM SAMPLE 76

APPENDIX C - EFFICIENCY FACTOR AND HEAT SINK CALCULATIONS

.....88

APPENDIX D - RESIDUAL STRESS EVALUATION 90

List of Tables

I. Computer Model Parameters 40

II. ESJ Typical Log Sheet 41

List of Figures

1. Schematic Layout of ESJ Equipment 42
2. Electroslag Typical Weld Structure(Ref. 35) 43
3. ESJ Thermal Profile - Calculated and Measured 44
4. Boundary Conditions 45
5. Nodal Arrangement 46
6. Model Flowchart 47
7. Stress Analysis Schematic Diagram 48
8. UBC Electroslag Unit 49
9. Cooling Shoe - Water Channels 50
10. Cooling Shoe Top View 51
11. Copper recess 52
12. Cooling Shoes in Position 53
13. Cooling Shoe Close-up - Water connections 54
14. Plate Electrode in Position 55
15. Aluminum Feeder 56
16. Electrode and Copper Stub 57
17. Run-in Copper Tabs 58
18. Constraining Rod with Strain Gauges 59
19. Strain versus Time Plot 60
20. Boxed I-Beam 61
21. Hardened 4340 Disc Spacer 62
22. Inferior I-beam Placement 63
23. Strain-gauge Set-up 64

24. Thermal Stress Curve 65

25. Thermal Stress Curve 66

26. ESJ Thermal Gradient 67

Acknowledgement

Sincere thanks to Dr. Alec Mitchell for his guidance throughout the duration of this work.

Thanks are also due to Dr. E. B. Hawbolt and fellow graduate students for innumerable helpful discussions.

The assistance of the technical staff, in particular Mr. E. Barry and Mr. G. Sidla is greatly appreciated.

The financial support provided by the Canadian International Development Agency and by Eletrometal Acos Finos S.A./Ministerio da Industria e Comercio - Secretaria de Tecnologia Industrial, Brasil is gratefully acknowledged.

A special thanks to Consuelo for her care and encouragement.

I. INTRODUCTION

1.1 Introduction

The manufacture of large steel forgings via the conventional route requires starting ingots having a low ingot-to-forging yield(30 to 60%) and a low equipment potential utilization time due to the heavy weights involved. Alternative production routes have, therefore, to be sought.

Several techniques have been proposed in an effort to present viable solutions. The MHKW(Midvale-Heppenstall-Klockner-Werke) process[1] is one whereby a conventionally cast ingot is trepanned and subsequently core remelted, thus improving the quality of the ingot central part through enhanced isotropic ESR properties. The B.E.S.T.(Boehler Electroslag Hot Topping) technique[2] is also a potential process for improving the ingot-to-forging yield.

A further promising route is the use of Electroslag Joining for welding two or more pieces of steel before forging to make a large preform or joining already forged products to their final

shape.

Russian workers have developed a method for joining large sections used in the manufacture of rotor forgings for atomic power station turbogenerators.[47] Four large section consumable electrodes were employed and the welding equipment used a bifilar configuration which is claimed to be very efficient. In this investigation it was concluded that the process would be applicable to the production of heavy rotor forgings using high alloy Cr-Ni-Mo-V steels and a comparative assessment was made of the fracture resistance of the weld and parent metal with good mechanical properties obtained. It was also found that preliminary and concurrent heating of the parts being joined were eliminated.

Little has been done as to the application of the process in the case of carbon steel forgings in the range 20-100 t, which represents the bulk of the open die forging market.[9] Here the main concern is with repeatability, reliability, ultrasonic testing and product qualification. In other words, the process behaves very similarly to the more conventional welding techniques and, therefore, must be carefully controlled to avoid defects.

The process is carried out with ease and relatively fast in one single pass and when compared with, for example, submerged-arc welding, time savings are significant. The resultant coarse

structure due to long thermal cycles is liable to produce lower mechanical properties and better equipment control and welding procedures are needed.

1.2 Process Description and Application

Electroslag Joining is one of the several applications of the Electroslag Remelting principle. It is a fusion welding process whereby heat is generated by Joule effect when an electric current passes through an electroresistive flux(slag). Both the tip of the electrode and the surface of the work are melted by heat coming from the slag source. The electrode molten droplets transfer by gravity to the weld pool by falling through the molten flux . As can be seen in Fig. 1, the axis of the joint is vertical but the welding is performed in a horizontal position. The remelted product is surrounded by the parent material and by cooling shoes either stationary or movable.

The most popular version of the process is the one employing flux-coated or bare wire electrode feeding as well as consumable or non-consumable electrode guides. In this case, the filler material(wire+guides) and the parent metal often have dissimilar compositions and when several wires are used,

depending on the thickness of the parts being welded, proper monitoring of the feeding system becomes rather critical.

The weld metal acquires a casting structure wherein the sizes and orientations of the grains are controlled by heat removal. The presence of long columnar grains is characteristic and four types of grain structures have been defined by Paton.[35] Because the process introduces a large amount of heat into the parts being joined, a large heat affected zone can be expected. Fig. 2 illustrates these microstructures. Segregation along the grain boundaries of these columnar grains can cause crack appearance as discussed below.

The typical slow cooling rates in the process when cooling from the austenite range form pearlite: the proeutectoid ferrite normally forms a network along the prior-austenite grain boundaries and Widmanstatten side plates that extend from the grain boundaries into the matrix.[5] Due to fast cooling, residual stresses are present in the weld and heat affected zone but are somewhat relieved in the longitudinal direction.

The use of plate electrode as filler metal has recently been considered and it is believed to enable more efficient heat transfer. Because the electromagnetic forces do not produce as stray fluid motions, slag velocities are slower(2 to 4 cm/s) and the total weld heat may be reduced by as much as 30% when plate electrodes are used instead of wire welding. Also the heat flux

to the base metal from the slag is more uniform.[6]

The hydrogen content of the steel has been found to decrease with increasing calcium fluoride content in the flux. A system containing CaF_2 + Al_2O_3 is recommended for effective hydrogen control.[7] Also the hydrogen content has been found to be larger at the weld start than elsewhere. To lessen this effect, as discussed below, proper pre-heating of the flux components was normal procedure throughout these experiments. A liquid slag start procedure should improve the hydrogen control even further, should this prove to be a problem.

Electroslag Welding and Electroslag Joining have usually been used to join heavy thickness, large welds and applied to the manufacture of generator rotors for the nuclear industry, to the on-site welding of thick vertical joints where Arc Welding could not be employed,[3 5] and to the construction of bridges, buildings and storage tanks.[4] High pressure vessels and heavy boiler drums used in power plants have also been fabricated.[3 5 8] Welding of forging presses and anvils up to 2000 X 2000 mm and of rolling mill frames as well as ship rudder parts has been performed.[4 3] Recently, main propulsion shafting and other machinery shafts for use in Classed Ships made by Electroslag Joining have been qualified under Lloyd's Register requirements.[3]

1.3 Previous Work

The theory of moving sources in welding(Arc Welding) heat conduction presented by Rosenthal[10] and the analytical modelling proposed by Rykalin[11] set basis for all subsequent work done in the field of weld modelling. Little attention has been given to the thermal stress calculations in Electroslag Joining except for some published Czech work[22 25] done with wire electrode welding.

The resulting complex equations from analytical studies on welds have always hindered a better understanding of the different processes, especially in studying thermal stresses[17]. Gray et al[20] have improved Okerblom's[12] theory of one-dimensional stress analysis based on a two-dimensional heat flow treatment and applied to thin gauge materials. Little experimental information was given which could be used to test the theory and it made use of in-plane curvatures rather than contractions. These authors have, however, succeeded in carrying out experiments intended to test the theory for longitudinal contractions.

With the ever increasing speed of modern computers, solution techniques have been devised which enable more accurate and faster calculations. The first attempt to make use of computers in analysing welding stresses dates as far back as 1961.[18] Masubuchi[17] reported some efforts being made at analysing transient longitudinal stresses during multipass welding of a heavy plate, but no results were given. The majority of experimental studies of thermal stresses during welding, however, has used materials in the thickness range of 0.30 mm to 25.4 mm(0.012" to 1"), which were all done using Arc Welding whilst experiments in the present work were performed using much thicker material. Nishida[21] reviewed several methods for calculating thermal stresses and compared theoretical results with experimental data, again working with thin materials.

Eriksson et al[30] have developed a hot-cracking test to assess the weld metal composition influence on the hot-cracking tendency in heavy Electroslag welds and have concluded that to avoid solidification cracking, the carbon content should be kept as low as possible and the Mn/S ratio should exceed 45. In this test, however, the stress fields are not known either in absolute terms or in relation to those present in heavy section welds.

There exist several other tests to evaluate weldability

cracking problems and two of them seem to be especially suitable for solidification cracking: Varestraint and Transvarestraint tests. They are the same in principle and operation, except for the direction of the applied strain with respect to the welding direction. They have not been applied to electroslag welding configurations.

Ueda et al[19] have developed a method for theoretical analysis of thermal stresses, taking into consideration effects of changes in modulus of elasticity, yield stress and the coefficient of linear expansion on the metal with temperature. At the instant of welding, a limited portion of the parts being joined such as the weld bead and the parent material close to the hot face is heated up to a very high temperature and thereafter cooled down to room temperature. As this thermal cycle proceeds, the temperature distribution changes with time and the mechanical performance of the welded assembly is also a function of temperature. It is, therefore, imperative to assess the temperature distribution during welding.

Pertsovskii et al[26] have calculated the thermal cycle in the heat affected zone during Electroslag Welding of thick steel plates and have realized that the nonuniform generation of heat in the liquid pool and complex pool outline, make it extremely hard to study the heat flow distribution at the boundary between solid and liquid phases. However, they have replaced the above

mentioned complex volumes by a collection of three linear heat sources at different levels in the pool for a semi-infinite system. The results presented seem to agree well with measured values and are applicable to CGESW(Consumable Guide Electroslag Welding).

More recently, Bacon[23] studied the heat flow in both systems(wire and plate electrode). High deposition rates, shallow slag depth requirements, smooth heating and cooling rates and greater degree of penetration are realized in Electroslag Joining as compared to wire electrode welding. Temperature distribution measurements and calculations done for the present project followed the same trend found by Bacon[23] and had similar heating and cooling rates, respectively 0.5 - 2.0°C/s and 0.2 - 1.0°C/s.(See Fig. 3)

1.4 Solidification Cracking

Work developed both by Brown et al[27] and by Phillips et al[28] have indicated that provided the same stress field is applicable, Electroslag Joining should not be more or less susceptible to solidification cracking than conventional welding. The critical welding speed which will ensure a sound weld has been defined by Semenov[29], taking into account thermal stresses and mainly the volume change during metallurgical

transformations. The technique consists in imposing a tensile stress on the solidifying region of a fully-constrained weld (which represents the worst case). According to these authors, stable welding voltage assures the correct penetration during the weld and together with the critical welding speed determine the proper shape factor(ratio of the weld gap to the metal pool depth) for a sound weld. With increasing heat input the depth of the metal pool increases sharply, the shape factor varies and the tendency to form cracks also increases.According to Makara et al[44], an increase in the weld voltage leads to improvement of the shape of the pool profile and results in crack tendency reduction. Bendis[43] has concluded that the most critical period during Electroslag Welding is when one-quarter to one-half of the joint is welded. The parameters that control the resistance of the weld metal to hot cracking as reported by Paton[35] are: chemical composition, rigidity of the welded joint and the shape factor. Brown et al[27], however, found no cracks when applying the suggested welding conditions given by Semenov et al[29] and even deliberately altered the Mn/S ratio to a value lower than the recommended minimum of 45 which according to Eriksson et al[30] should have resulted in solidification cracking. It is,therefore, clear that Electroslag Welding(wire electrode) behaves quite differently with respect to stress build-up as compared to Electroslag Joining(plate electrode)

The high heat input observed in Electroslag Welding which keeps the slag pool in the molten condition can be very

effective in avoiding the uptake of hydrogen from moisture but it is known to enhance conditions leading to cracks in the welds. The possibility of solidification cracking(hot cracks) exists both in the weld metal(solidification cracking) and in the heat affected zone(liquation cracking).[33] Steels are known to fail in a brittle manner at temperatures close to the melting point and this behaviour is ascribed to incipient melting of solute rich regions in the steel which results from grain boundary segregation or microsegregation during solidification.[46] For continuous casting steels with 0.25% to 1.0% C the brittle range starts at 40°C below the solidus temperature as reported by Weinberg.[42] When the deformations in this temperature range exceed the deformation capacity of the metal a hot tear develops.[33] Lower melting point secondary phases such as sulphides and oxides at the heat affected zone at the grain boundaries fuse locally and produce a weaker bonding that fails under the effect of shrinkage stresses causing what is known as liquation cracking. In both cases, however, rupture of the metal occurs in an intergranular form, contrasting with typical lower temperature, intracrystalline path cold cracks, resulting mainly from hydrogen embrittlement.[48] Rymkevich et al[32] have pursued the determination of the brittle temperature range in Electroslag Welding of carbon steels and found it to be 1380-1450°C.

1.5 Present Objectives

As described above, conditions in the welds leading to cracks are realized in the process despite the improvements experienced by a higher heat input and suitable welding flux in the plate electrode technique. An understanding of the nature and extent of solidification cracking and, therefore, of the proper welding conditions has prompted the need for further studies of the thermal stresses produced in the process.

II. MATHEMATICAL MODELING

The inherent difficulties associated with performing experimental work, especially in the case of stress determination in welds, make it all the more interesting to use a model in order to study how the process behaves. The following pages contain the development of a computer program which was used to calculate the thermal stresses realized during the Electroslag Joining of thick blocks, based upon a temperature profile input.

Weld cracking in Electroslag Joining appears to be caused by thermal stress-field induced by nonuniform temperature changes. It is essentially a question of how much heat flows through the plates being joined. Although radiation and convection take place while Electroslag Joining, conduction is the dominant heat transfer mode in the blocks, except during hot topping when radiation and convection start playing a more significant role.

According to Liby et al.[34] two aspects of heat flow need to be considered: heat generation in the slag and heat conduction through the parent blocks. The former is assigned a melting point temperature as the starting value for calculations in the first time step of the model and from the second time step on,

it is calculated for every time step, taking into consideration the electrode latent heat, heat conductivity and density. The latter will constitute the underlying principle based upon which the temperature distribution will be determined.

2.1 Temperature Distribution Calculation

2.1.1 Assumptions

The general heat conduction Fourier equation in two dimensions is thought to describe the phenomena involved and is used to calculate the thermal profiles. In order to solve it, several assumptions had to be made so that the boundary conditions could be properly applied:(See Fig. 4 and Fig. 5)

i) No-flux boundary condition at the top of the slag. According to Paton[35] only 1.3% of the total heat is radiated to the surfaces and 1.2% is actually lost throught radiation to the atmosphere.

ii) Symmetry axis -- because the welding process is symmetrical, a no-flux boundary condition is thought to be a valid assumption.

iii) Block walls -- the internal walls were also assumed a

no-flux condition as the heat radiation mentioned in i) is negligible.

iv) All the heat reaching the slag-metal interface leaves it and flows to the blocks being welded.

v) Positions in the block away from the hot face(fusion line) are considered to be at room temperature and the temperature of the heat source (slag) to be the melting point temperature for carbon steel(1520°C.)

vi) Physical properties were considered to be constant and the electrode latent heat was taken into consideration. Such an assumption is not too far from reality as the energy coming from the idealized heat source(slag+metal pool) actually reaches electrical equilibrium in light of the fact that, if the right volume of slag is chosen, the welding equipment performing the weld operates in a stable manner. Values for Cp, k and are listed in Table I.

vii) The heat source(slag + metal pool) travels "indefinitely" along the height of the block, although an unsteady state model was used to predict the thermal profiles.

viii) As in the case of welding large assemblies, no heat flow in the z direction is assumed.

ix) Symmetry is invoked and the modelling is built on one side of the joining assembly as illustrated in Fig. 4.

2.1.2 Derivation Of Equations

The two dimensional heat conduction equation

$$\frac{\partial^2 T}{\partial x^2} + \frac{\partial^2 T}{\partial y^2} + \frac{q}{k} = \frac{\rho\, Cp}{k} \frac{\partial\, T}{\partial\, t} \qquad (1)$$

Where: T = temperature

t = time

q = heat flux

k = heat conductivity

ρ = density

Cp = specific heat

Letting $\alpha = \rho\, Cp/k$ and knowing that there is neither heat generation nor consumption in the blocks($q/k=0$), equation (1) becomes:

$$\frac{\partial^2 T}{\partial x^2} + \frac{\partial^2 T}{\partial y^2} = \frac{\alpha\, \partial T}{\partial t} \qquad (2)$$

Equation (2) is solved numerically subjected to different boundary conditions(See Appendix A).

2.1.3 Numerical Solution

Using a heat balance approach for an interior node, the governing equation was expressed in finite difference form as:(See Fig. 2)

For $1<i<IM-1$

$1<j<IN$

For the first half time step:

$$\frac{-\alpha}{\Delta x^2} T^*_{i-1,j} + \left(\frac{2}{\Delta t} + \frac{2\alpha}{\Delta x^2} \right) T^*_{i,j} - \frac{\alpha}{\Delta x^2} T^*_{i+1,j} = \frac{2}{\Delta t} T^n_{i,j} + \tag{3}$$

$$+ \frac{2\,\alpha (T^n_{i,j+1} - T^n_{i,j})}{\Delta y_j (\Delta y_j + \Delta y_{j+1})} - \frac{2\,\alpha (T^n_{i,j} - T^n_{i,j-1})}{\Delta y_j (\Delta y_j + \Delta y_{j-1})}$$

Similarly for the second half time step:

$$\frac{-2\,\alpha}{\Delta y_j (\Delta y_j + \Delta y_{j-1})} T^{n+1}_{i,j-1} + \left(\frac{2}{\Delta t} + \frac{2\,\alpha}{\Delta y_j (\Delta y_j + \Delta y_{j+1})} + \frac{2\,\alpha}{\Delta y_j (\Delta y_j + \Delta y_{j-1})} \right) T^{n+1}_{i,j} -$$

$$- \frac{2\,\alpha}{\Delta y_j (\Delta y_j + \Delta y_{j+1})} T^{n+1}_{i,j+1} = \frac{2}{\Delta t} T^*_{i,j} + \frac{\alpha}{\Delta x^2} (T^*_{i+1,j} + T^*_{i-1,j} - 2\,T^*_{i,j}) \tag{4}$$

and solved numerically by using an Implicit Alternate Dir ection Finite Difference method in 2-D. The other nodes were determined similarly(See Appendix A). The unsteady state conditions, typical of Electroslag Joining(mainly the heat distribution in the blocks) calls for an implicit method such as the I.A.D.F.D., making the solution independent of any stability criteria. This technique solves a 2-D problem by using a 1-D approach in one direction(implicit by columns) for the first half time step and again a 1-D solution for the other direction (implicit by rows) and second half time step.[36] A tridiagonal system of equations is simultaneously solved without any restrictions as to the spatial and time increments. Fig. 6 presents the main flowchart for the model.

2.2 Thermal Stress And Strain Calculation

Stresses appear as a result of nonuniform heating of the elements of a body which cannot expand freely. In Electroslag plate joining the heating and cooling rates are typically low but, as the process is a long one, the total heat input is rather large and, therefore, bound to create thermal stresses and strains.

Considering a rectangular beam of depth 2h, thickness TH and length L(See Fig. 7), assuming L to be much larger than the other dimensions(See Appendix C) and knowing that T = T(x), a simple model was used to calculate thermal stresses and strains. Because the beam is considered thin(mid-section plane in Fig. 4) a plane stress assumption is made:

$$\sigma_{zz} = \sigma_{yz} = \sigma_{xy} = 0 \tag{5}$$

$$\sigma_{xx} = \sigma_{zx} = 0 \tag{6}$$

and

$$\sigma_{yy} = \sigma_{yy}(x) \tag{7}$$

For the analytical solution of the resulting two-dimensional problem which by applying equation (6) becomes a one-dimensional problem(equation (7)) all bounding surfaces are free of traction except the end faces y=+L/2 and y=-L/2 and the following equations satisfy equilibrium and compatibility conditions[38]:

Stress Components:

$$\sigma_{yy} = -\alpha E T + \frac{1}{2H} NT + \frac{3x}{2H^3} MT \quad (8)$$

$$\sigma_{xx} = \sigma_{zx} = 0 \quad (9)$$

Strain Components:

$$\varepsilon_{yy} = \frac{1}{E}\left(\frac{NT}{H} + \frac{3x}{H^3} MT\right) \quad (10)$$

$$\varepsilon_{xx} = \frac{-\nu}{E}\left(\frac{NT}{H} + \frac{3x}{H} MT\right) + \left(\frac{1+\nu}{1-\nu}\right)\alpha T \quad (11)$$

Where NT is the integral of α ETdz from -h to +h and MT is the integral of αETzdz from -h to +h

The values of E(Young's Modulus) were calculated as a function of temperature according to the experimental results published by Minakami et al.[37] for carbon steel. The integrals which appear in the analytical expression above were calculated numerically and were used in equations (8) and (10) to calculate the thermal stresses in the y-direction for each corresponding nodal temperature thus, covering the entire height being welded.

A sample of the computer program used to calculate the stresses and strains is shown in Appendix B.

2.3 Computer Production Runs

The thermal stress calculations were performed for several welding conditions (different temperature distributions), all of which simulated real joinings. Provisions were made in the program to allow for changes in the furnace parameters which would affect the final welded stress state. Thus, varying the heat input namely amperage and voltage, produced a different welding speed which, in turn, caused a different stress distribution. Since the process is very stable electrically, the welding velocity was considered to be constant throughout the model. The initial temperature conditions for the weld region is replaced every subsequent time step by a new temperature calculated upon a heat balance performed at the fusion boundary. Only a small amount of energy released by the electrode melting effectively goes into the joining blocks. The efficiency factor F used to determine how much of the available incoming energy flows through the blocks gives an indication of the thermal efficiency of the process.

A massive heat extraction is performed by the copper and aluminum cooling shoes. This very efficient heat sink absorbs

approximately 50% of the energy available and little is lost as radiation energy, except until the very end of the process.

III. EXPERIMENTAL WORK

3.1 Furnace Design

The equipment used for all runs was the U B C Electroslag facility as shown in Fig. 8. This unit can cast steel up to 1 t in weight and operates on AC. The furnace power supply is a 250 KVA step-down transformer which is connected to a 600 V primary single phase line. This dry type transformer operates with a high voltage of 600 V and a low in the range of 25-60 V, AC current of up to 8000 A.

The electrode feeding system consists of a) an electrode holder carriage which slides on aluminum rails inside the furnace framework(Fig.8) and is suspended from b) an electrode drive carriage coupled to a variable speed reductor that enables speeds from 0 to 163 mm/min. The operational parameters are readily monitored from several instruments in a control panel. More detailed information on the furnace design is given elsewhere.[39]

3.2 Cooling Shoe Design

Electroslag Joining is fundamentally similar to Electroslag

Remelting.The readily noticeable difference lies in the remelted product: in the joining process the parent material is part of the heat extraction system whilst in plain remelting the product is completely surrounded by water-cooled copper crucibles. Heat flows by conduction through the blocks and a substantial portion is extracted via the cooling shoes. Therefore, this part of the set-up plays a significant role in controlling the directional solidification.

The design used features rectangular aluminum slabs 25.4 mm X 254 mm X 1066.8 mm(1"X10"X42"), with three 11 mm deep cooling groves(channels) per shoe on the outer aluminum section(See Fig. 9) copper and which was coupled to the inner copper slab(Fig. 10).This recess in the copper part increases the surface area contact and enables proper positioning of the electrode. Considering that the copper has a higher heat conductivity, it resulted in a rather efficient heat removal, thus ensuring proper cooling and good wear resistance. Fig 12 and 13 show the shoes in place and a close-up. The water enters through the bottom, circulates through the channels and leaves through the top.

3.3 Electrode And Slag Preparation

The electrode(i.e., the filler metal) in Electroslag Joining has the same composition(whenever possible even from the

same steel shop run) as the parent material being welded. This assures chemical homogeneity and weld repeatability.[8] The commercial carbon steel used for both the filler and parent material was ASTM A36 whose composition is:

C=0.29%

Mn=0.90%

Si=0.15%

P=0.04%

S=0.05%

A typical electrode section would be two 152.0 mm(6") X 19 mm(3/ 4") X 2930 mm(115"),38 mm thick, as illustrated in Figs. 14 and 15. It is connected to a water-cooled stub that is perfectly aligned with the furnace frame.(Fig. 16) A small rod 25 mm(1") in diameter and 152.4 mm(6") long is welded to the bottom of the electrode so as to have a faster weld start.

Two 152 mm X 457 mm X 914 mm plates weighing approximately 500 kg each were used in the experiments.

The welding flux used was of composition: 55F/15/15/15, i.e.,

CaF_2=55% CaO=15% Al_2O_3=15% SiO_2=15% (% in weight)

and pre-heated at a temperature of about 600°C in order to

avoid any moisture retention. A total of 7.0 kg per weld was enough to maintain stable welding conditions.

3.4 Weld Set-up And Constraining

All the weld preparation was done on a movable colorlith platform that slides on a monorail(Fig. 8). A protective layer of asbestos is put on top of the colorlith where the starter plates are positioned. In order to ensure proper weld penetration since the start of the weld and also to make set-up and stripping operations more efficient, run-in water-cooled copper sumps, as shown in Fig. 17 were used. At the top of the blocks close to the weld, 76.2 mm(3") run-out sumps were tack-welded to extend the block height and thus, accommodate the slag volume past the joining sections.

The cooling shoes are held in position by braces which are tightened on to bolts welded onto the blocks(Fig.12). The blocks were set 100 mm apart(which is the recess length) (Fig. 11). An air setting high temperature mortar(SAIRSET) is spread along the shoe sides touching the blocks to provide a safe sealing against any possible slag and/or metal leakage. When this was completed the assembly was ready to be placed in the welding position. At this stage the electrode was inserted in the weld gap using the overhead crane, aligned and tightened

to the stub.

When a weld is fully-constrained and no cracking is observed, it may be a good indication that the weld can accommodate contraction movements and will likely be a sound one. Therefore, constrained set-ups were prepared so as to produce a weld crack. Initially an I-beam with I(inertia moment) of approximately 23 in^4 was thought to be strong enough to stand up to the pressures in the system and was positioned at the top of the blocks. A sturdier I-beam was needed and it was prepared so as to have an inertia moment of 126 in^4, as shown in Fig. 20. The weld on the I-beam did fail as the set up became rigid and the strain gauges were unable to record the actual strain undergone by the weld metal.(See Fig. 19) At this stage it was realized that as the weld went on the system(blocks being joined + weld region) became more rigid below the welding point(metal pool), to an extent that the welded I-beams could not take the pressure and, therefore, did not properly constrain the weld. It was then thought that if the constraining rods were placed at the bottom a lower system stiffness would be effected thus, enabling a stronger constraining capability which would result in a weld crack. The I-beams were arc welded on to the ends of the blocks away from the hot face, initially at the top and later at the bottom. A rod 76.2 mm(3") in diameter, 965.2 mm(38") in length and slightly tapered off at the ends was positioned in free compression restraining the parts from closing in(See Fig. 18). Fig. 20 and Fig. 21 show the boxed I-

beam with increased inertia moment and the hardened 4340 disc spacer to avoid any localized deformation.

The strain-gauges were set on both constraining rods and monitored by a Transducer/Strain Indicator 8-channel STRAINSERT - Model TN8C. For correct measurements a gauge factor was used and the apparatus was operated in full bridge mode.

Fig. 22 presents the same set-up described above except for the fact that the constraining rods were positioned at the bottom. This way, the same constraining rigidity would be experienced whilst the assembly stifness would not be as large as when the rods were placed at the top and, therefore, the rod strength would be comparable to the weld strength. Once the strains are known, the stresses can be calculated as the rods remain in the elastic region.

3.5 Sequence of Operation - Welding Procedure

After the electrode is properly aligned, a mixture of calcium fluoride and steel shavings(the 'compact') is positioned on top of the starter plate and under the electrode tip; the

cooling system is checked for leaks and the pre-heated flux is poured into the gap. Initially an arc is struck and the small 25 mm diameter rod is readily melted. At this stage,some of the flux starts to melt and soon the volume of slag is such that no more arcing occurs and heat is generated by slag resistance only. Table II shows the furnace parameters for a typical Electroslag Joining experimental run. Aluminum deoxidation was effected throughout all the runs at a rate of 1 g/min.(See Fig. 15)

3.6 Residual Stress

After the weld was cooled down to room temperature, residual stress measurements were performed at the top of the assembly in the parent metal, in the heat affected zone and in the weld. The equipment used was supplied by Photolastic Inc., and the results were arrived at by using the Blind Hole Drilling Method.[45] Fig. 23 shows the schematic strain gauge set-up.

3.7 Temperature Measurements

Chromel-alumel thermocouples were placed in the block to measure temperatures in order to compare them with the

model.(Fig. 3) The results obtained as well as the penetration depth predicted agreed well with the observed values.

IV. DISCUSSION AND RESULTS

The Russian and Czech work developed in Electroslag Welding(wire electrode) had indicated that hot cracks were associated mostly with the weld chemical composition leading to transformational volume changes which would cause defects and that there existed a critical height range wherein cracks were more prone to appear. In their work it was never made clear whether the thermal stress field had been fully understood or even investigated. The magnitude of the stress fields in ESJ was not defined and even in a qualitative sense was not known.

The first attempts to study thermal stresses during plate electrode welding in this work, revealed that a great amount of the stress was being relaxed as the heat source travelled along the weld height. The large heat input(1.7 kW/cm), typical of this process, creates a rather broad temperature field(heat affected zone) capable of absorbing the high stresses that develop. Further experimentation confirmed the inability of the I-beams and rods to effectively constrain the blocks at the top and the fact that the thermal field was accommodating the deformations.

A much shorter weld was made with the constraining rods positioned at the bottom. The proposal was that, as mentioned above, the weld strength at a smaller height in terms of weld

cross-sectional area would be comparable to the area of the rods and, therefore, the latter would be able to take up the weld stresses. It was found that even after that procedure the weld did not present any cracks, the thermal field having presumably relaxed them even in a true fully-constrained weld.

Both welds(constrained at the top and at the bottom) were thoroughly tested ultrasonically and no cracks were found. After that they were sent out to be inspected by radiography. The pieces were exposed to Co-60 radiation for approximately 15 hours and again no indication of cracks was found.

The thermal stresses predicted by the model and calculated for several welding conditions were consistent with experimental observation. In Fig. 24 the conditions set for the computer run were the same as the ones undergone by the actual joining experiment. It is noted that during most part of the weld the resulting thermal stresses for different distances away from the block hot face are tensile in nature. When the liquid pool approached the end, new boundary conditions were imposed to account for radiation and convection whereupon compressive stresses start to appear, subsequently, inducing tensile stresses underneath the liquid pool where metal is solidifying. If those compressive stresses are higher than the material yield strength, then they should induce the high tensile stresses that would lead to cracks.

In order to investigate further the results above, a run with identical welding conditions(except for the weld height which was doubled up) was tried and the same trend was again observed.(See Fig. 25). In other words, should the computed values for the stresses at the end of of the weld be exceedingly high for a particular set of welding conditions then, by adjusting the latter a less severe stress field would result which, in turn, provided enough penetration is effected, could in principle indicate the optimum welding conditions to produce a crack-free weld.

The residual stresses remaining in the system after cooling to room temperature were measured and found to show tensile stresses develop during or after welding. The residual stresses in all three positions(parent metal, heat affected zone and weld metal) were tensile and below the material yield point. See Appendix D.

Based on the modelling results and on the actual experiments performed, it is possible to say that the characteristic broad thermal field of Electroslag Joining in the parts being joined enhances thermal stresses in the weld(as well as in the heat affected zone) which are relaxed by the thermal field to a considerable extent as the weld progresses.

These findings seem to contradict the results presented by the Czech literature on Electroslag Welding cracks. It has been observed and predicted that the cracks in Electroslag Joining, if at all present, will always occur at the top of the joint when compressive stresses start mounting due to thermal contraction, wherever the top may be.

If the Czech/Russian approach to predicting hot cracking were to be followed, then a steel which transforms at high temperatures would have cracks when a steel of low transformation temperature would not. These workers have predicted that high alloy grades such as Ni-Cr-Mo-V forgings do not crack when carbon steels do. If so, the steel used for the present study should have resulted in solidification cracking once it is already a 'good' crack-former in terms of transformation volume changes.

V. CONCLUSIONS

1) Considering the theoretical calculations and experimental evidence, it can be said that Electroslag Welding and Electroslag Joining differ quite significantly as to the thermal stress build-up and hot crack tendency. It is clear that the dissimilar thermal profiles experienced in each of these processes result in different stress fields. The resulting crack formation tendency is therefore quite different.

2) The residual stress measurement confirms the results predicted by the model and observed experimentally. The residual stress values are below the weld yield strength level and, therefore, no cracks were detected in ESJ under conditions which would have produced cracks in ESW.

3) Electroslag Joining is more applicable to the welding of heavy gauge forgings than Electroslag Welding due to its intrinsic features. It should probably be regarded more as a shop fabrication technique than as a field welding process.

4) A simple mathematical model was developed which enables the semi-quantitative visualisation of the thermal and stress trends realized during welding

5) The theoretical predictions can be used when assessing the application of this heavy thickness joining method.

VI. SUGGESTIONS FOR FUTURE WORK

1) Produce a weld having a narrow thermal field, i.e., a narrow weld gap, using wire electrode with narrow consumable guide in order to verify the thermal stress field approach to explaining hot cracks in this kind of weld.

2) Use higher alloy steels having different lower transformation temperatures under the same conditions cited in 1) to check on the influence of volume change in crack forming tendency.

3) Develop a more sophisticated mathematical model in order to be able to arrive at more accurate values when evaluating stresses. Such an approach would involve a lengthy and complex finite element thermal stress analysis coupled with experimental support in relation to the boundary conditions.

BIBLIOGRAPHY

1. Austel,W.;Heyman, H. and Maidorn, Ch., 6th International Vacuum Metallurgy Conference,San Diego, Ca., 1979, p. 747-756

2. Machner, P., 6th International Vacuum Metallurgy Conference, San Diego, Ca., 1979, p. 757-773

3. Vieira, E. M. and Guimaraes, A. A., Internal Report, Eletrometal Acos Finos S.A., Sumare, SP Brasil, 1982

4. Raman, A., Weld. J., vol. 60, (12), Dec. 1981, p. 17-21

5. Schilling, C. G. and Benter, W. P., National Cooperative Highway Research Program - Report 201 Transp. Res. Board, NRC, Washington, DC, May 1979

6. Dilawari, A.; Eagar, T. W. and Szekely, J., Weld. J., vol. 57, (1), 1978, p. 24s-30s

7. Masumoto, N. et al., Yosetsu Gakkaishi, vol. 46, (12), 1977, p. 869-875

8. Naganathan, S.; Screenivasalu, A. and Rao, A. S., Weld. J., vol. 52, (11), 1973, p. 125s-234s

9. Vieira, E. M. and Mitchell, A., Metals Technology, Oct. 1981, p. 405-410

10. Rosenthal, D., Trans. ASME, vol. 68, 1946, p. 849-866

11. Rykalin, N. N., "Calculation of Heat Flow in Welding", translated by Z. Paley and C. M. Adams, US contract number UC-19-060-3817, 1951

12. Okerblom, N. O., "The Calculations of Deformations of Welded Metal Structures", translated by DSIR, HMSO, London, 1958

13. Eregin, L. P. and Malai, A. E., Svar. Proiz., vol. 10, 1978, p. 26-27

14. Williams, N. T.; Smith, C. J. and Toft, L. H., Proceedings of the International Conference on Residual Stresses in Welded Construction and their Effect, The Welding Institute, London, Nov. 1977

15. Asai, Y. and Nakamura, U., "Electroslag Welding of Steel Slabs with Plate Electrodes", Nippon Steel Co., Nagoya Works, 2nd International Symposium of the JWS, Osaka, 1975

16. Prokhorov, N.N. et al.,Svar.Proiz., vol.1,1972, p. 2-4

17. Masubuchi, K., Proceedings of the International Conference on Residual Stresses in Welded Construction and their Effect, The Welding Institute, London, Nov. 1977

18. Tall, L., Weld. J., vol. 43, (1), 1964, p. 10s-23s

19. Ueda, Y. and Yamakawa, T., Trans. of the JWS, vol. 2, (2), Sept. 1971, p. 90-99

20. Gray, T. G. F. and Wickramasinghe, D. M. G., Welding Research International, vol. 8, (5), 1978, p. 409-421

21. Nishida, M., Master Thesis, MIT, March 1976

22. Becka, J. and Kupka, I., Zvaranie, vol. 25, (3), 1976, p. 72-77

23. Bacon, W. G., Ph.D. Thesis, UBC, 1979

24. Silva, A. C., Metl 560 Project, UBC, 1978

25. Becka, J., Zvaranie, vol. 29, 1970

26. Pertsovskii, G. A. and Pugin, A. I., Avt. Svarka, vol. 6, 1963, p. 14-23

27. Brown, R. and Mitchell, A., Steel Seminar 1980, UBC, Sept. 1980

28. Phillips, R. H. and Jordan, M. F., Metals Technology, Aug. 1977, p. 396-405

29. Semenov, V. M.; Gel'man, A. S. and Rymkevich, A. I., Svar. Proiz., vol. 11, 1973, p. 49-50

30. Eriksson, L. and Ostensson, B., J. Scan. Met., vol. 2, 1973, p. 282-284

31. Pense, A. W.; Wood, J. D. and Fisher, J. W., Weld. J., vol. 60, (12), Dec. 1981, p. 33-42

32. Rymkevich, A. I.; Gel'man, A. S. and Semenov, V. M., Svar. Proiz., vol, 10, 1973, p. 10-11

33. Homberg, G. and Wellnitz, G., Schweissen un Schneiden, vol. 27, (3), 1975, p. 90-93

34. Liby, A. L.; Martins, G. P. and Olson, D. L., "Modeling of Casting and Welding Processes", Conference Proceedings, The Met. Soc. of AIME, Rindge, NH, Aug. 1980, p. 161-196

35. Paton, B. E., "Electroslag Welding", A W S, N. Y., 1962

36. Carnahan, B.; Luther, H. A. and Wilkes, J. O., "Applied Numerical Methods", John Wiley & Sons, 1969

37. Minakami, H. et al.,Tetsu-to-Hagane, vol. 63, 1973, s562

38. Boley, A. and Weiner, J. H., "Theory of Thermal Stresses", John Wiley & sons, Inc., 1960

39. Sidla, G. and Mitchell, A., "The Design, Construction and Operation of an ESC Installation", Special Report to DREP/DSS, Vancouver, BC, June 1980

40. Frost, R. H. et al., Weld. J., Jan. 1981, p. 1s-6s

41. Mosny, J. and Slabon, I., Proceedings of an International Conference on Welding Research related to Power Plant, U. of Southampton, England, Sept. 1972, p. 456-463

42. Weinberg, F., Met. Trans. B, vol. 10B, June 1979, p. 219-227

43. Bendis, A., Zvaranie, vol. 16, (10), 1967, p. 365-370

44. Makara, A. M.; Gotal'skii, Yu. and Nuvikov, I. V., Avt. Svarka, vol. 8, (4), 1955, p. 3-12

45. Redner, S., "Measurement of Residual Stresses by Blind Hole Drilling Method", Bulletin TDG-5, Photolastic Inc., May 1974

46. Weinberg, F., Met. Trans. B, vol. 10B, Dec. 1979, p. 513-522

47. Paton, B. E. et al., Proceedings of a Conference on ESR, The ISI , U. of Sheffield, Jan. 1973, p. 105-112

48. Graville, B. A., "The Principles of Cold Cracking Control in Welds", Dominion Bridge Company, Ltd., Montreal, 1975

Table I - Computer Model Parameters

TMP=1520.0 (Deg C)
INITIAL TEMP= 25.0 (Deg C)
TIME STEP= 30.0 (s)
SPECIFIC HEAT=0.1070 (cal/g.C)
DENSITY= 7.860 (g/cm**3)
CONDUCTIVITY=0.0740 (cal/cm.s.C)
DX= 2.0 (cm)
HEAT FACTOR= 0.142
HEAT SOURCE DEPTH=12.000 (cm)
PRINT CYCLE= 600.0 (s)
END OF CALCULATION= 4200.0 (s)

DY=	0.5	1.0	1.0	1.0	1.0	1.0	3.0	3.0	3.0	3.0
DY=	3.0	3.0	3.0	3.0	3.0	3.0	3.0	3.0	3.0	3.0
DY=	3.0	3.0	3.0	3.0	3.0	3.0	3.0	3.0	3.0	3.0

NUMBER OF DIVISIONS IN X-DIRECTION = 50

NUMBER OF DIVISIONS IN Y-DIRECTION = 30

WELDING PARAMETERS:

WELD GAP= 9.5 cm THICKNESS= 15.0 cm

CURRENT= 5000.0 A VOLTAGE= 33.0 V

ELECTRODE SURFACE AREA= 57.9 (cm**2) WELD GAP AREA= 154.8 (cm**2)

LATENT HEAT= 65.0 (cal/g)

HOT TOPPING TIME = 3990.0(S) AIR TEMPERATURE = 30.0(DEG C)

HOT TOP CURRENT= 5000.0A HOT TOP VOLTAGE= 33.0V

WELDING VELOCITY= 0.023 (cm/s)

Table II - ESJ Typical Log Sheet

Time (s)	NMT	Prim (A)	Sec (A)	Volt (V)	MS (rps)	WT (Deg. C)
300	1468	320	4800	34	19	11.0
500	2118	330	5000	34	19	11.5
700	2881	330	5000	34	20	11.5
1000	4042	330	5000	34	21	11.5
1400	5631	330	5000	34	21	11.5
1700	6839	340	5100	33	21	12.0
2200	8847	340	5000	34	21	13.0
2400	9672	330	4900	33	21	13.0
2700	10987	340	5000	33	21	13.0
3000	12275	340	5000	33	21	13.0
3400	14058	330	4900	33	21	13.0
3700	15451	330	4900	33	21	13.0
4000	16805	310	4700	34	21	13.0

NMT = Number of Motor Turns
MS = Motor Speed
WT = Water Temperature

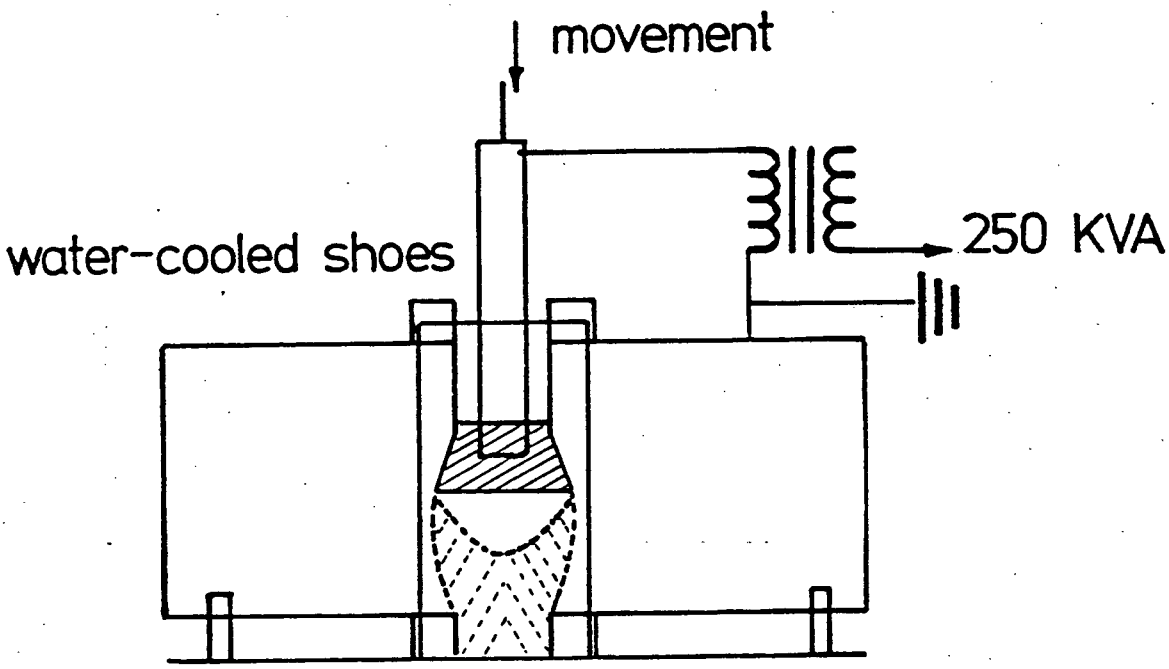

Figure 1 - Schematic Layout of ESJ Equipment

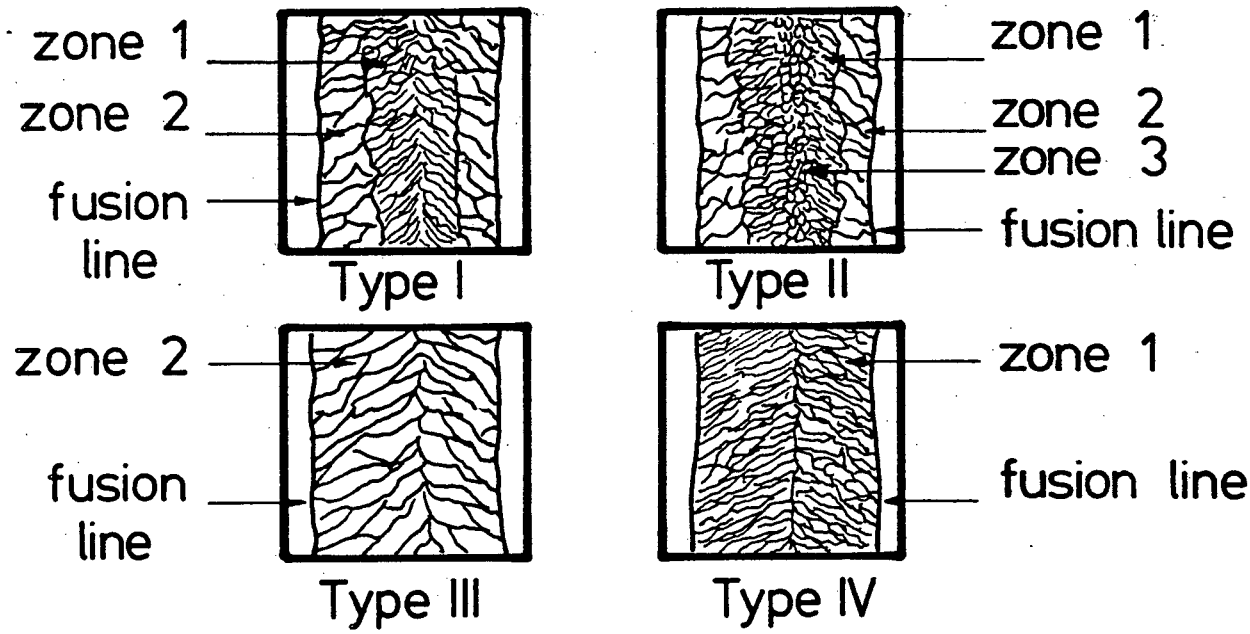

Figure 2 - Electroslag Typical Weld Structure(Ref. 35)

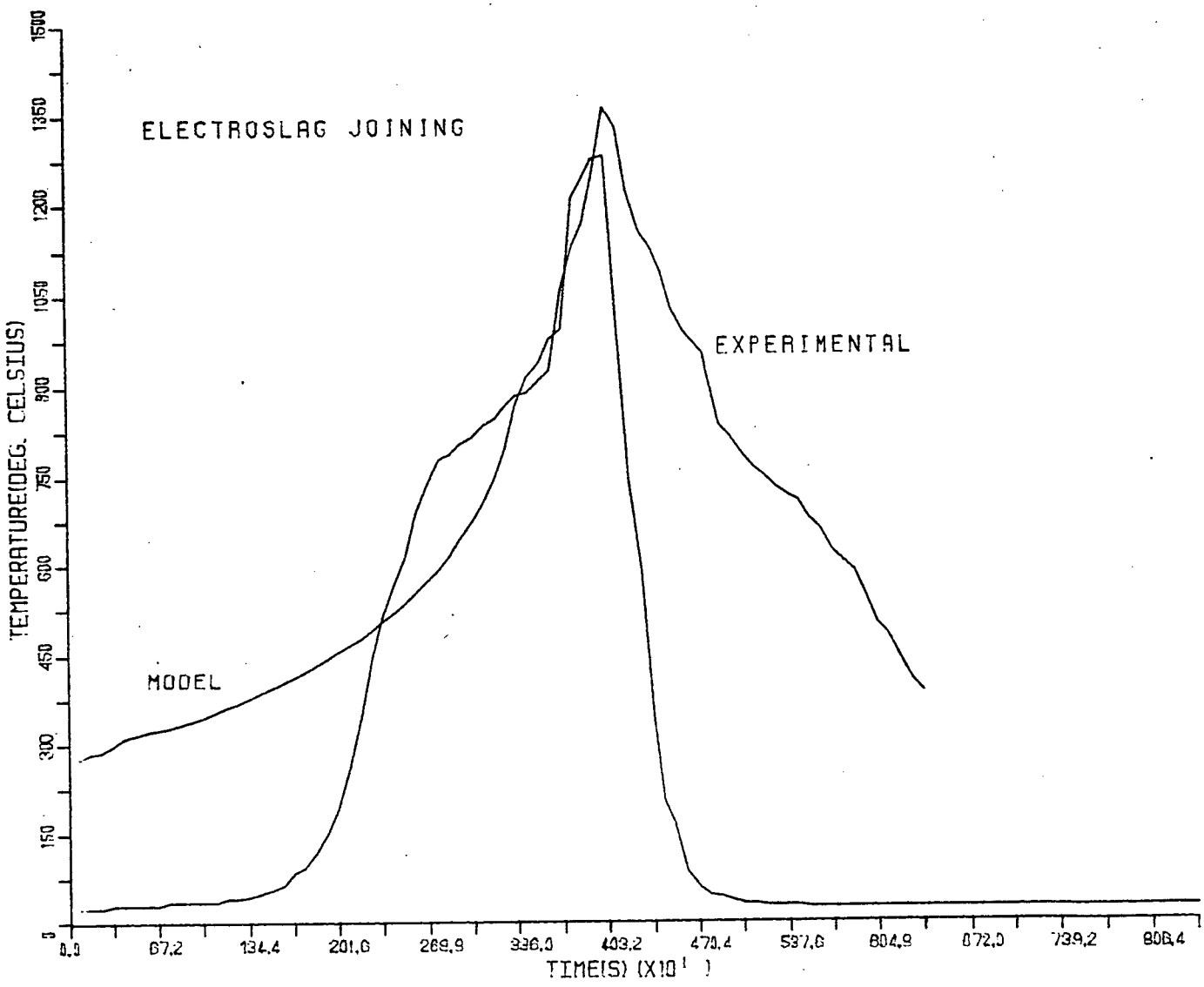

Figure 3 - ESJ Thermal Profile - Calculated and Measured

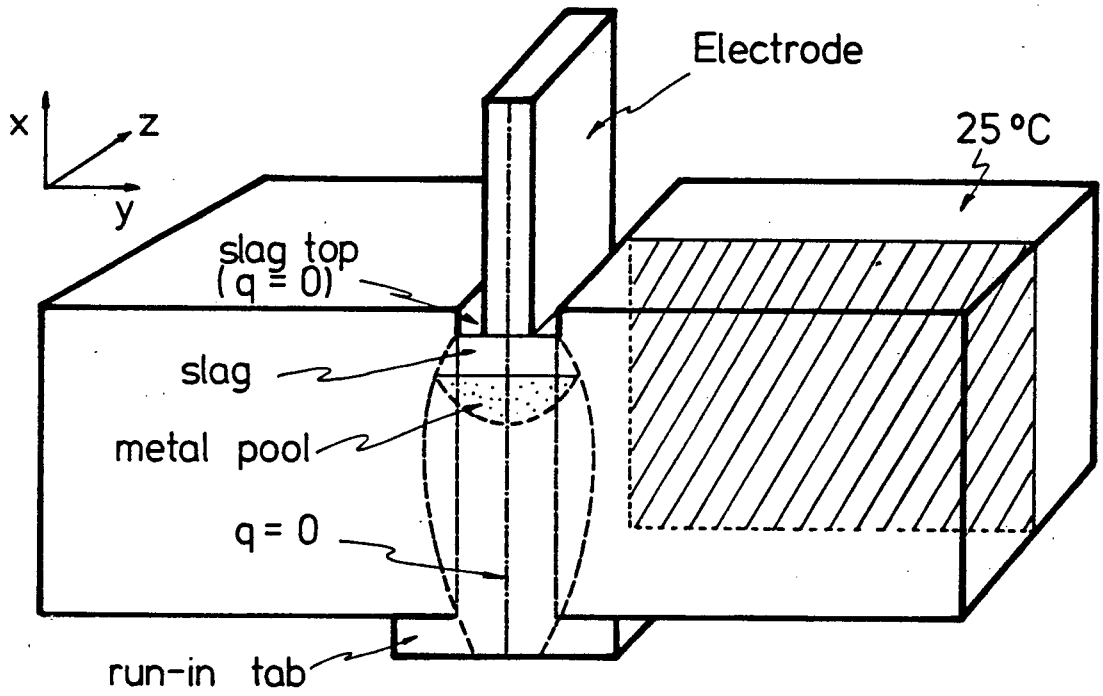

Figure 4 - Boundary Conditions

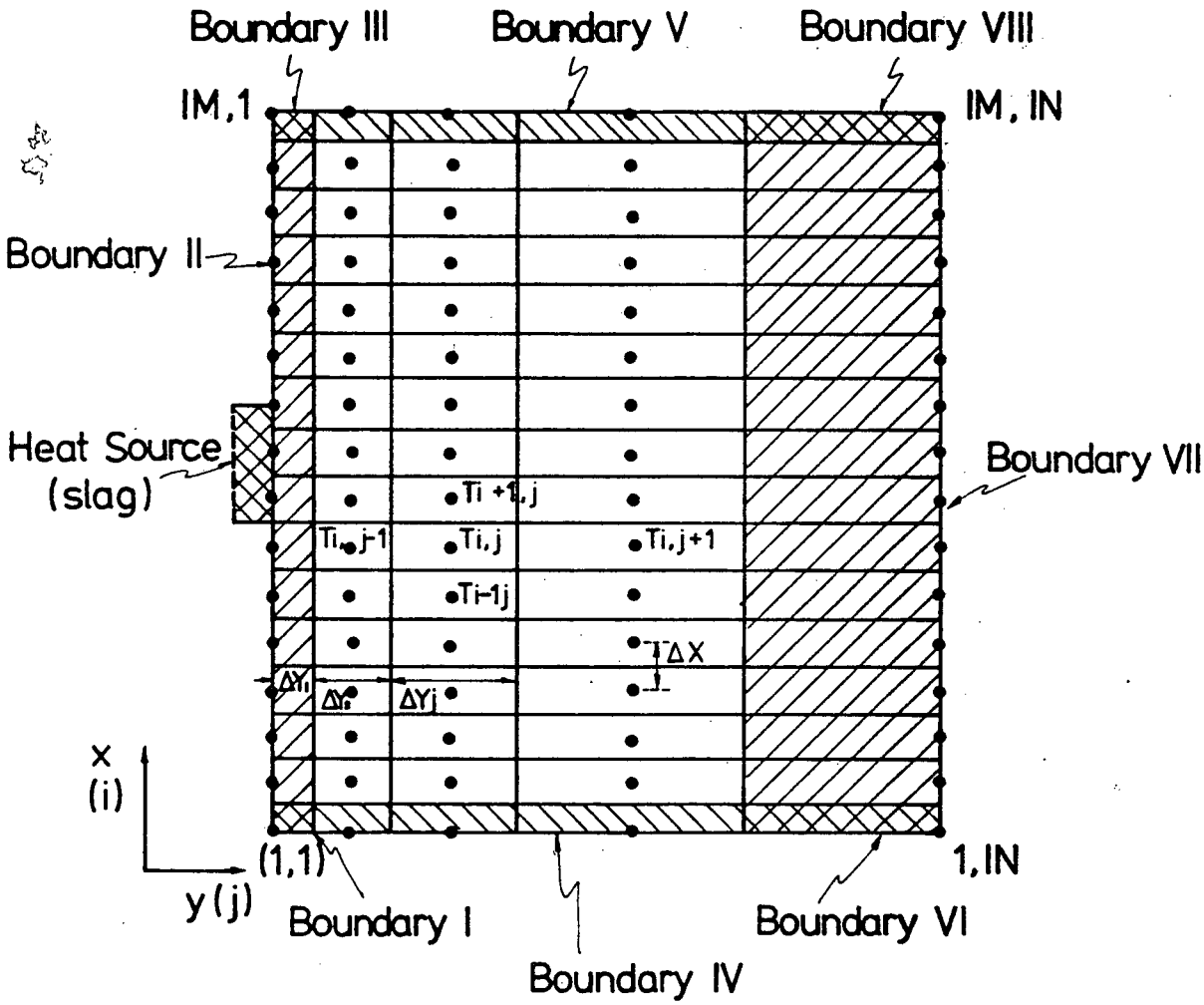

Figure 5 - Nodal Arrangement

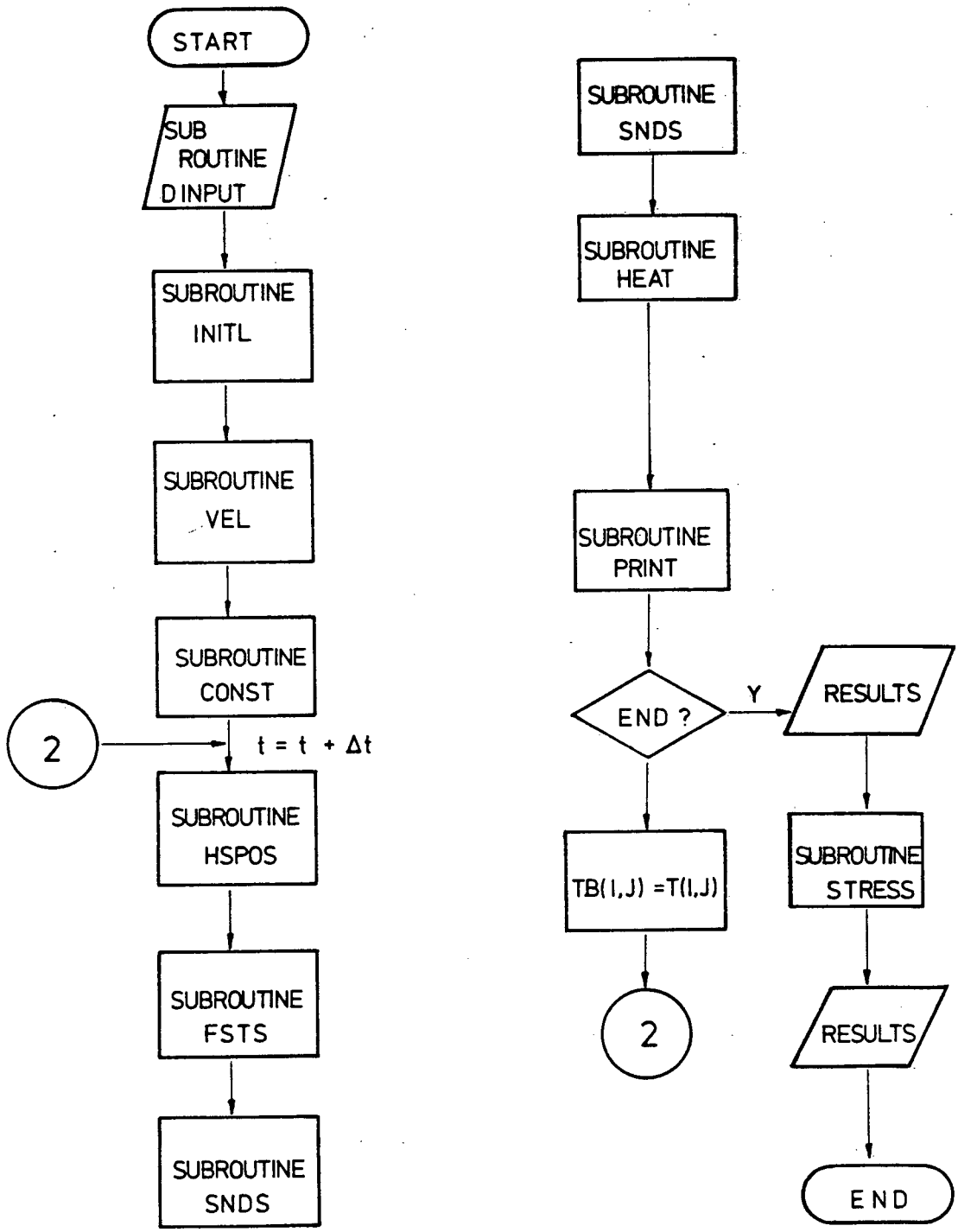

Figure 6 - Model Flowchart

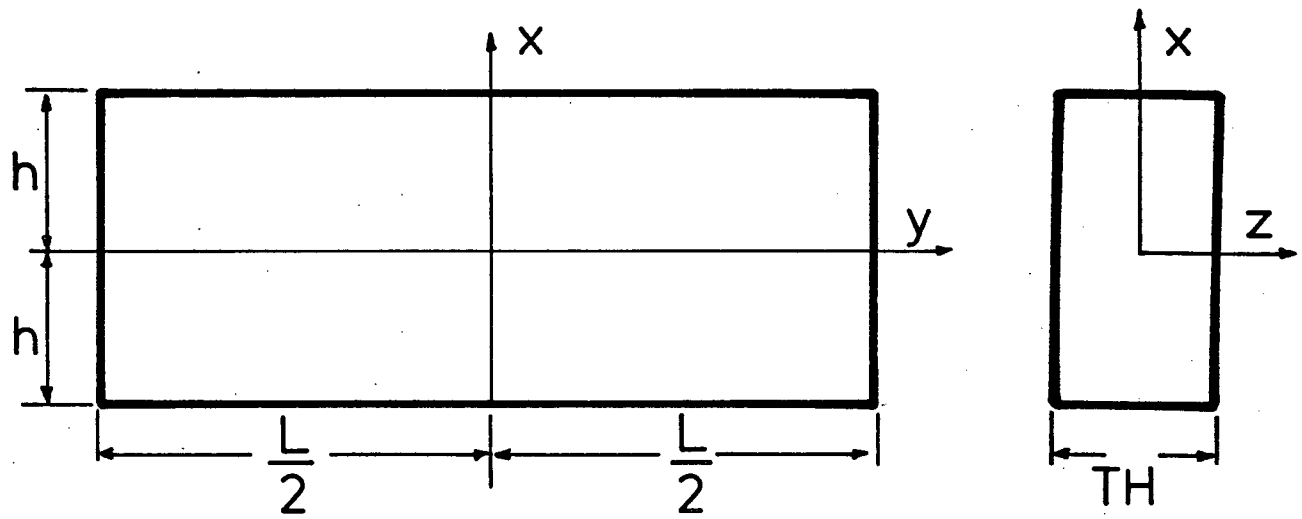

Figure 7 - Stress Analysis Schematic Diagram

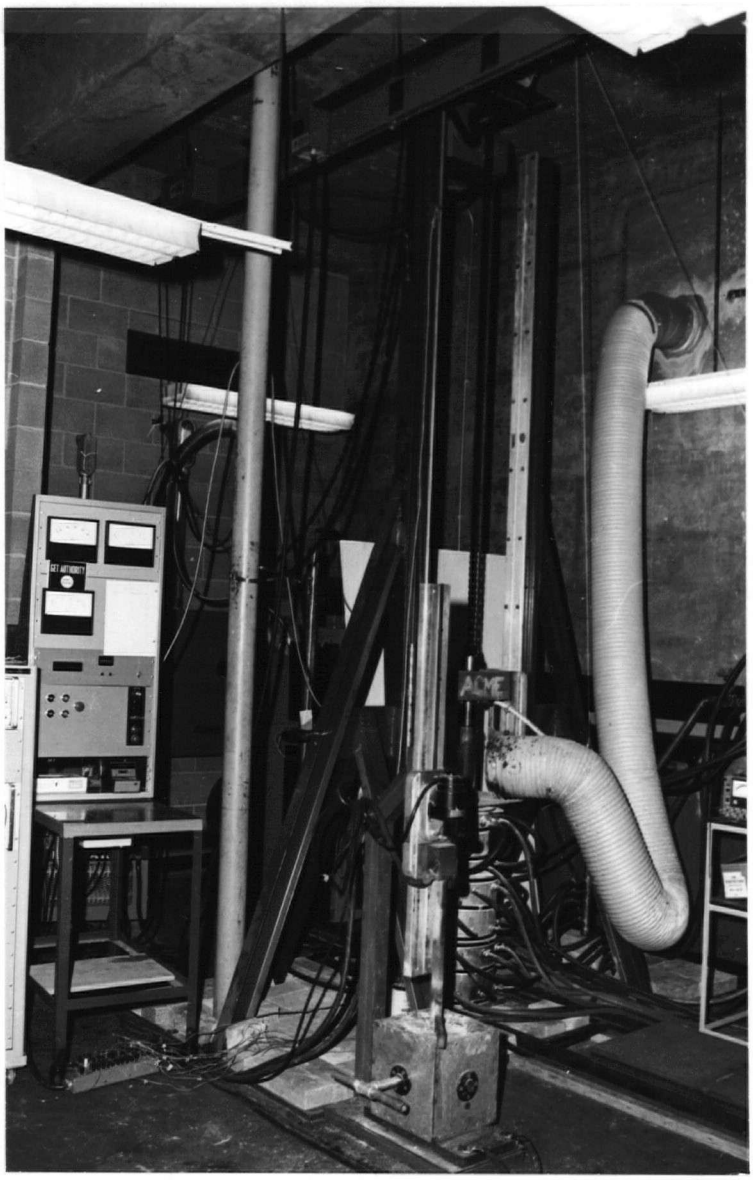

Figure 8 - UBC Electroslag Unit

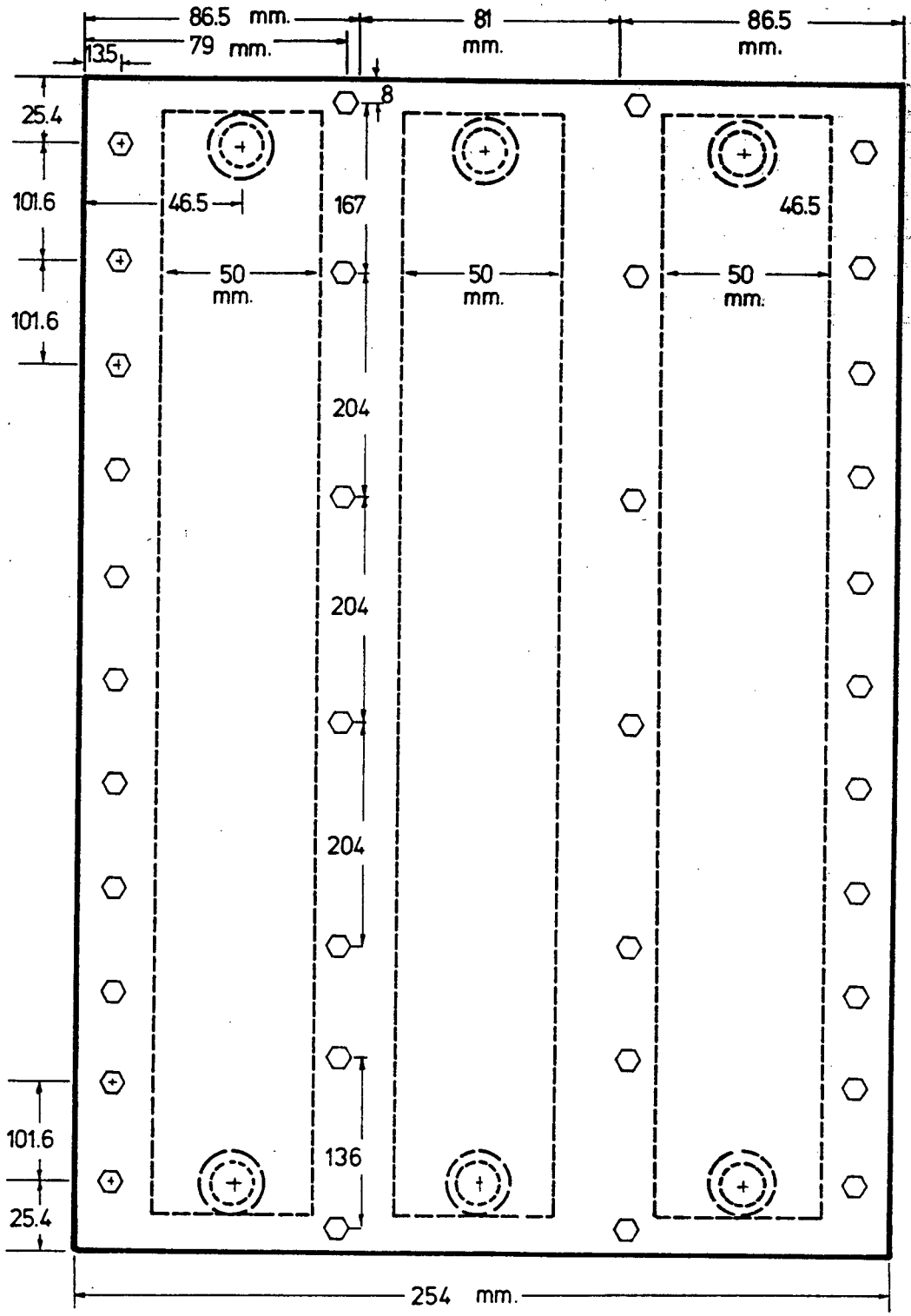

Figure 9 - Cooling Shoe - Water Channels

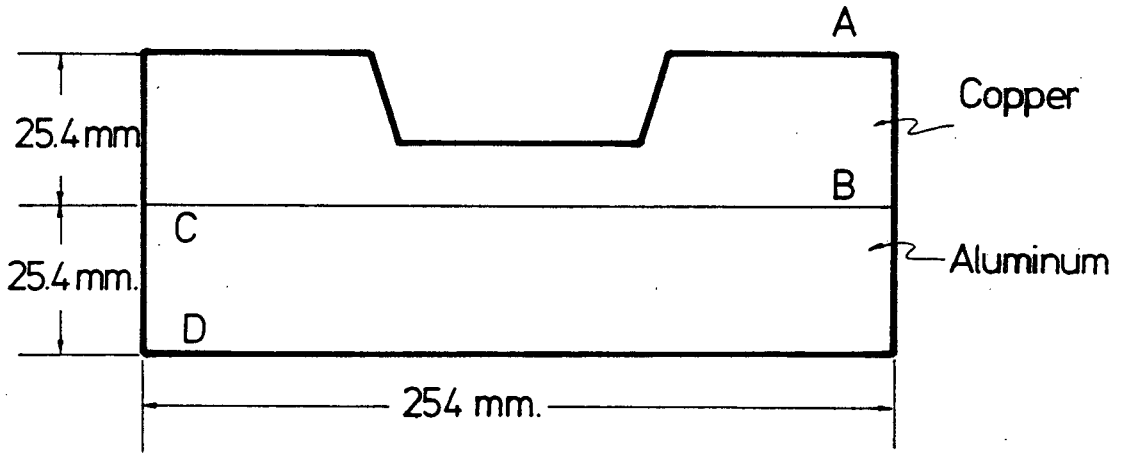

Figure 10 - Cooling Shoe Top View

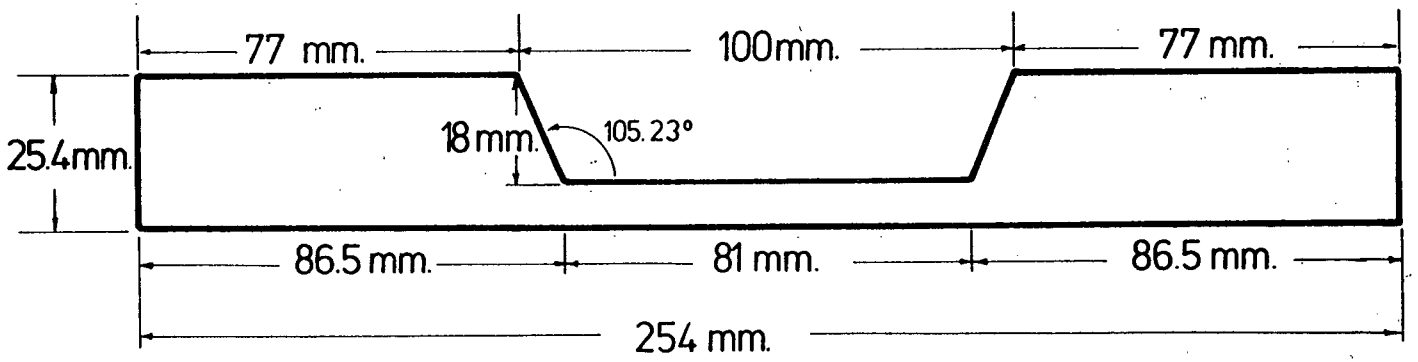

Figure 11 - Copper recess

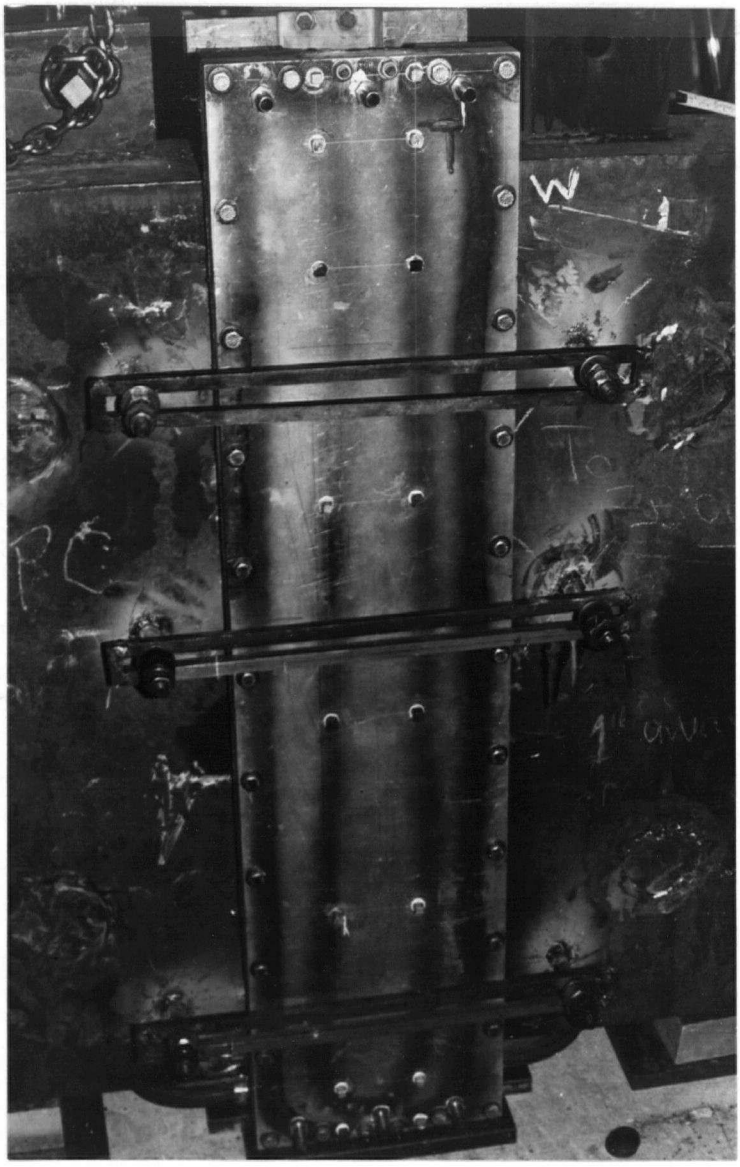

Figure 12 - Cooling Shoes in Position

Figure 13 - Cooling Shoe Close-up - Water connections

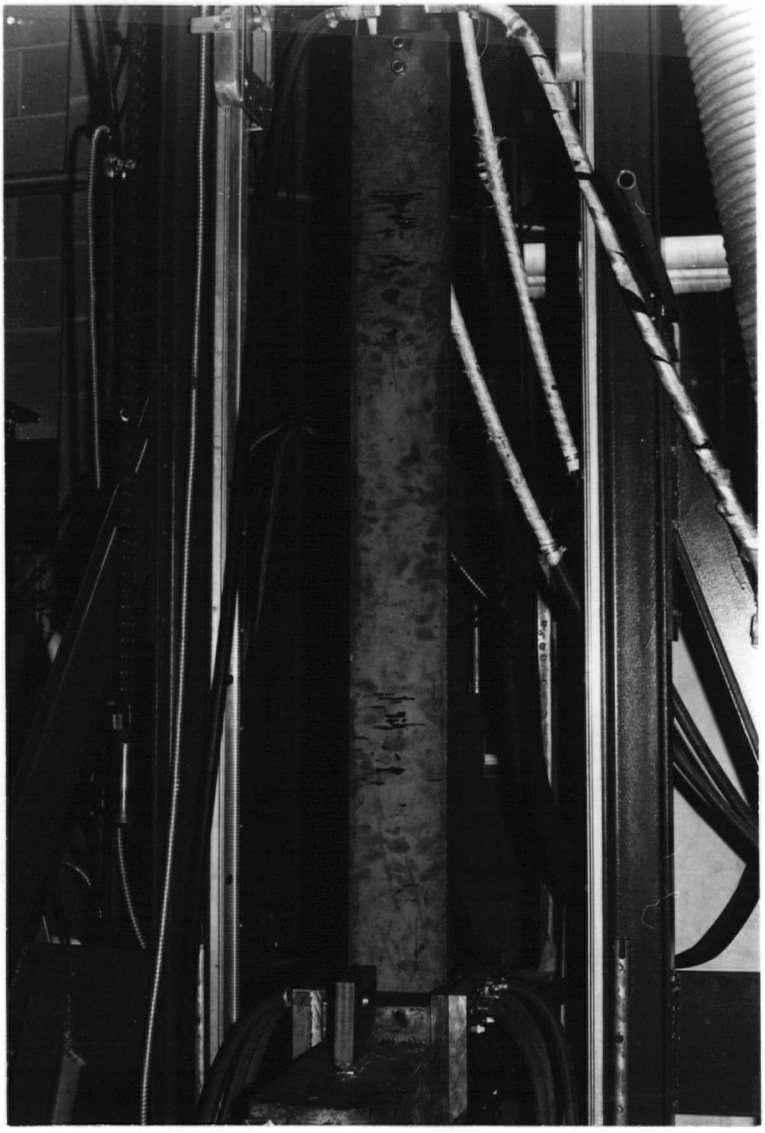

Figure 14 - Plate Electrode in Position

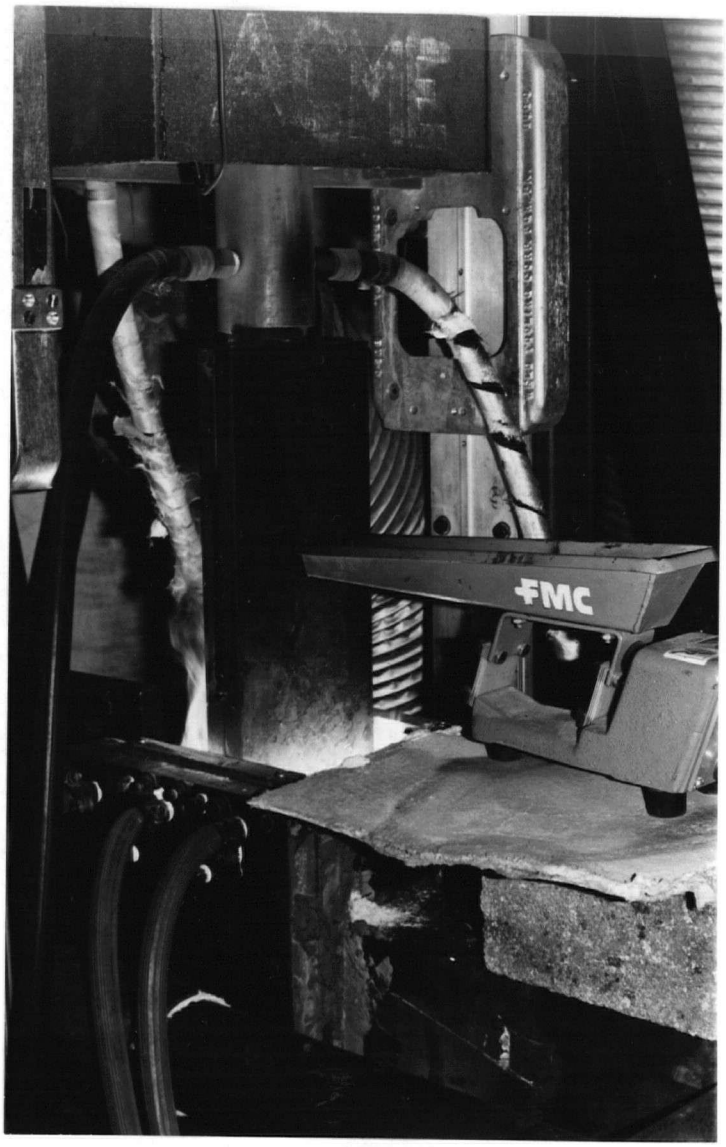

Figure 15 - Aluminum Feeder

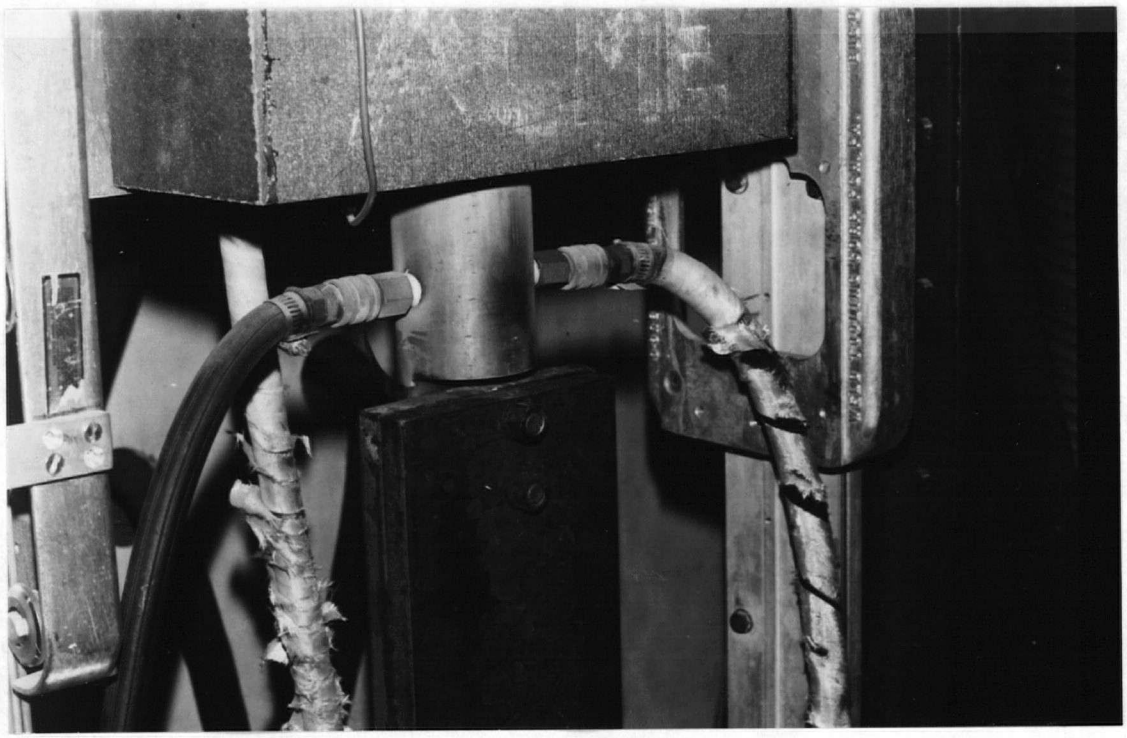

Figure 16 - Electrode and Copper Stub

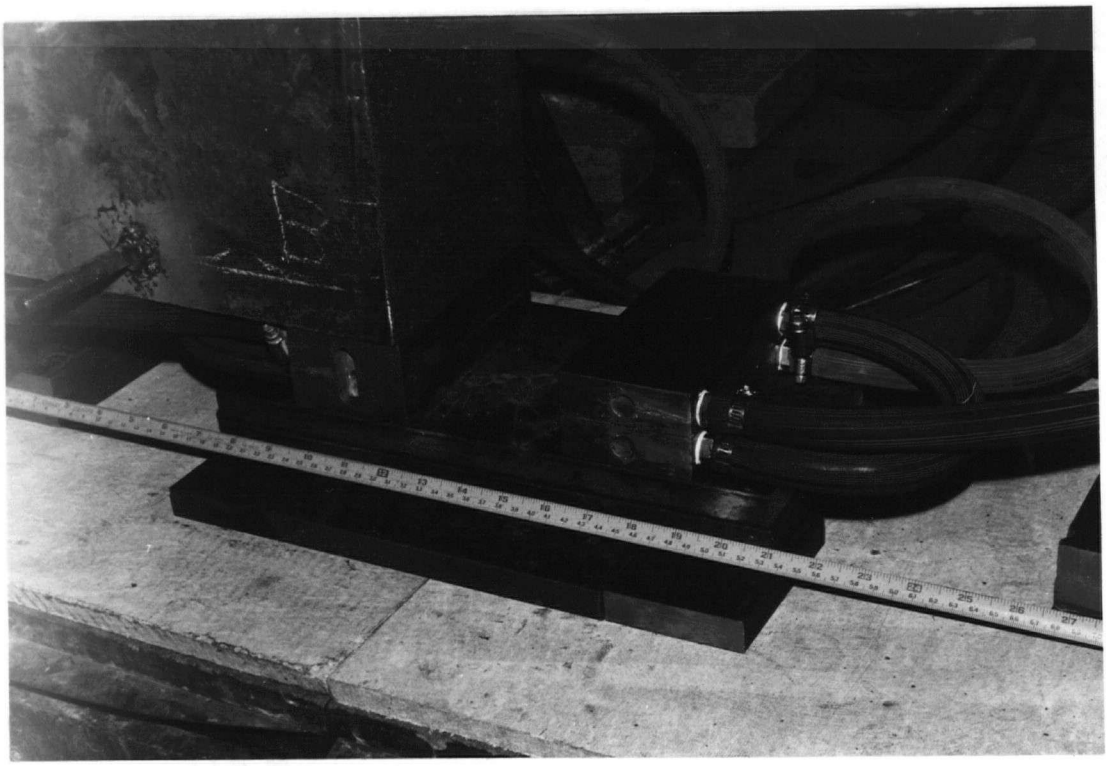

Figure 17 - Run-in Copper Tabs

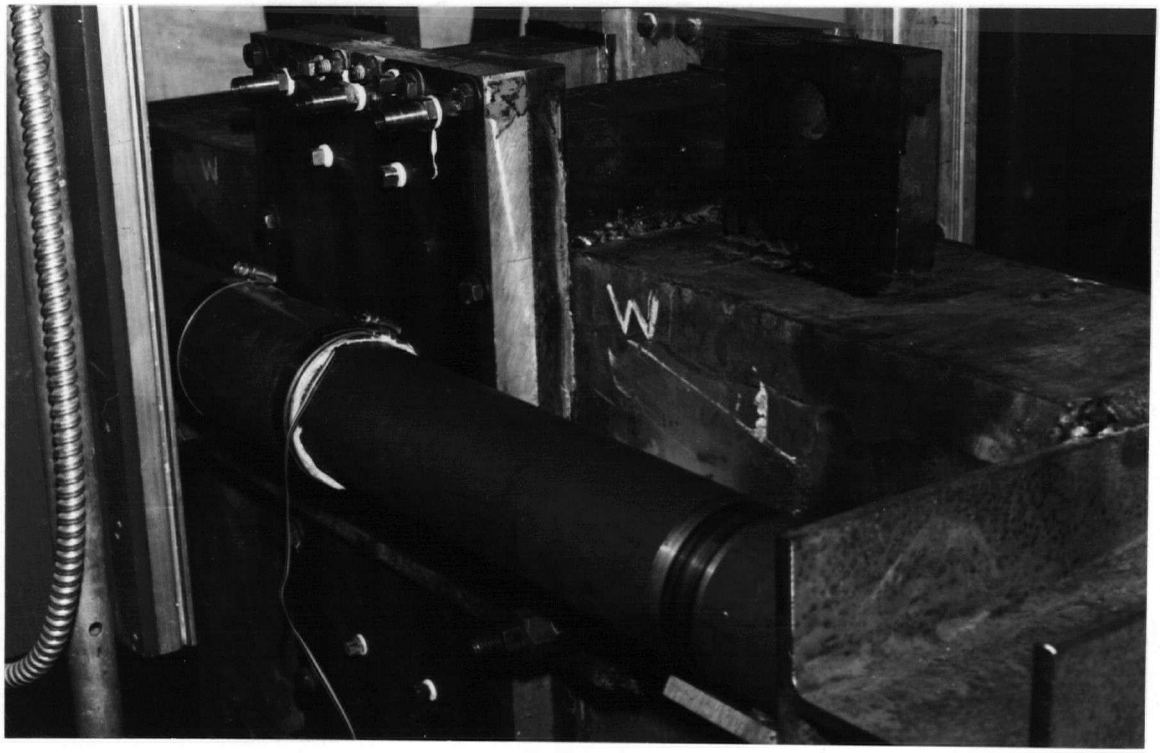

Figure 18 - Constraining Rod with Strain Gauges

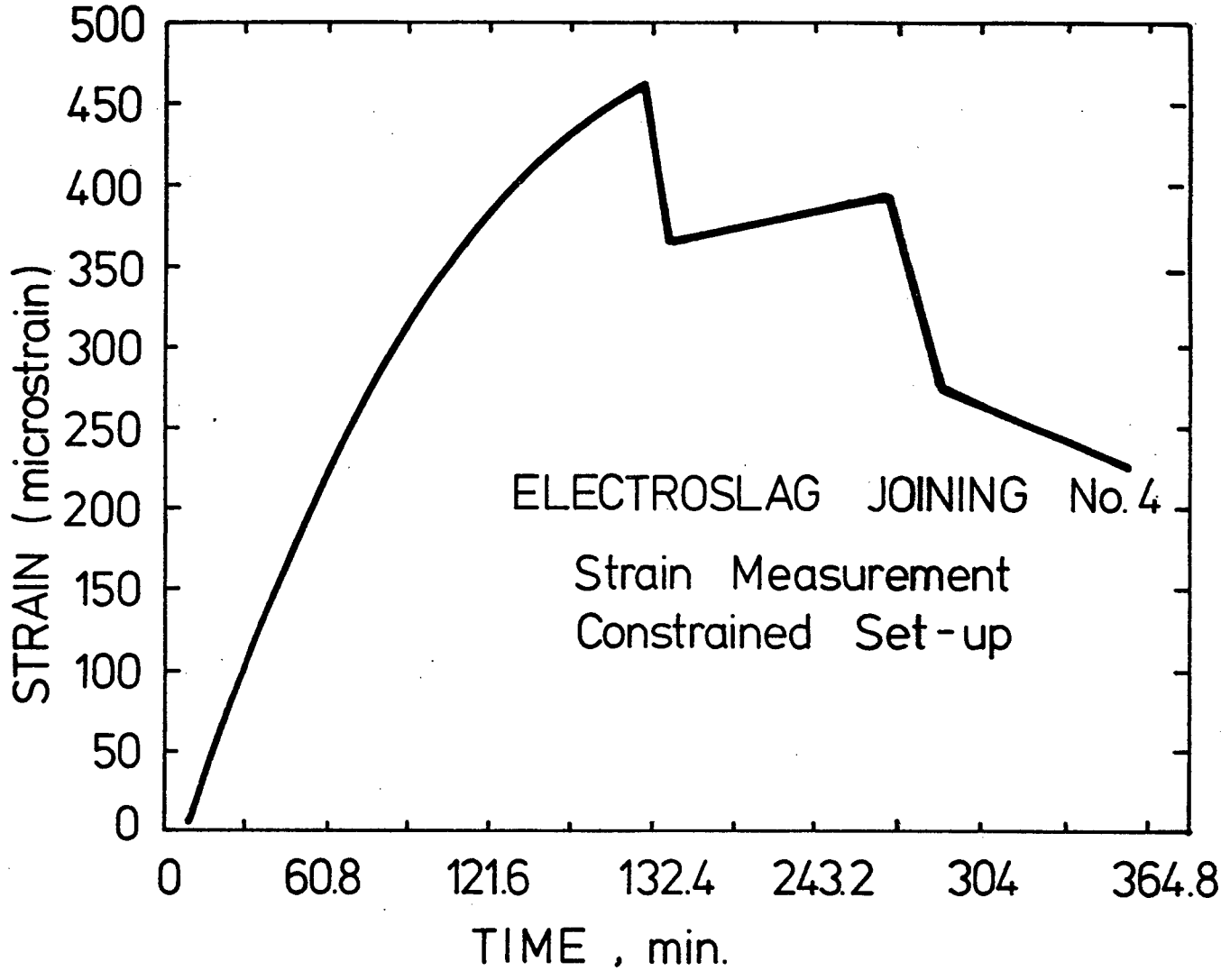

Figure 19 - Strain versus Time Plot

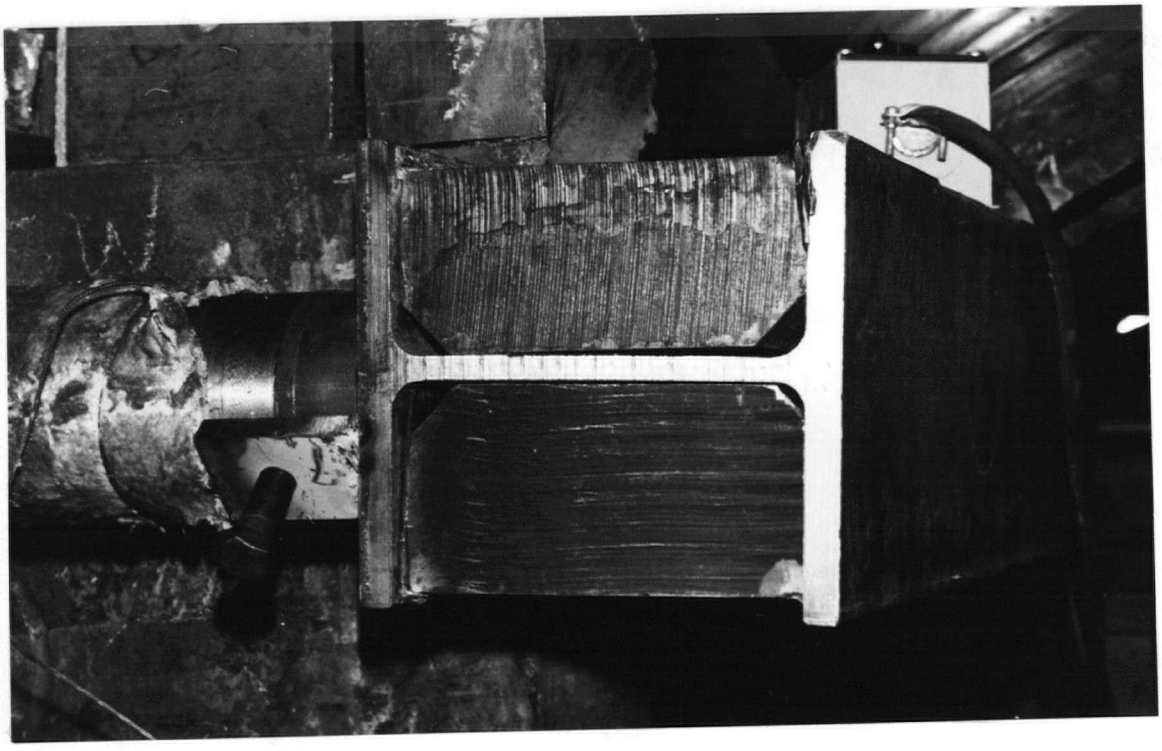

Figure 20 - Boxed I-Beam

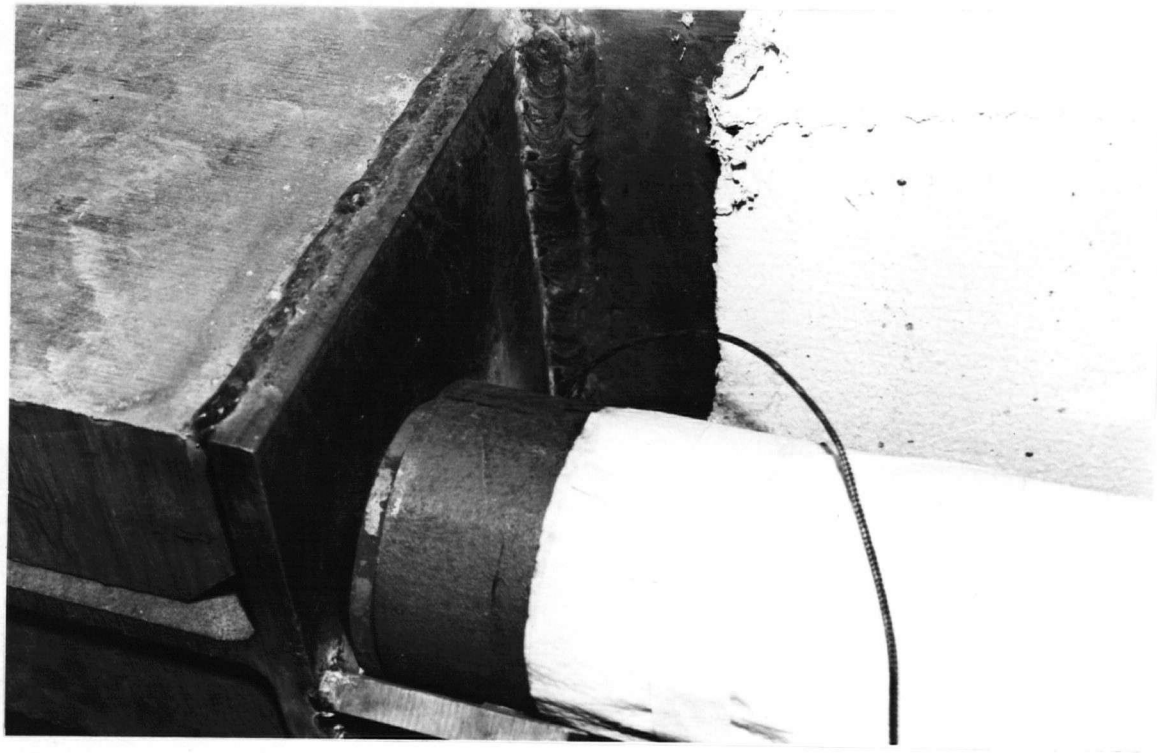

Figure 21 - Hardened 4340 Disc Spacer

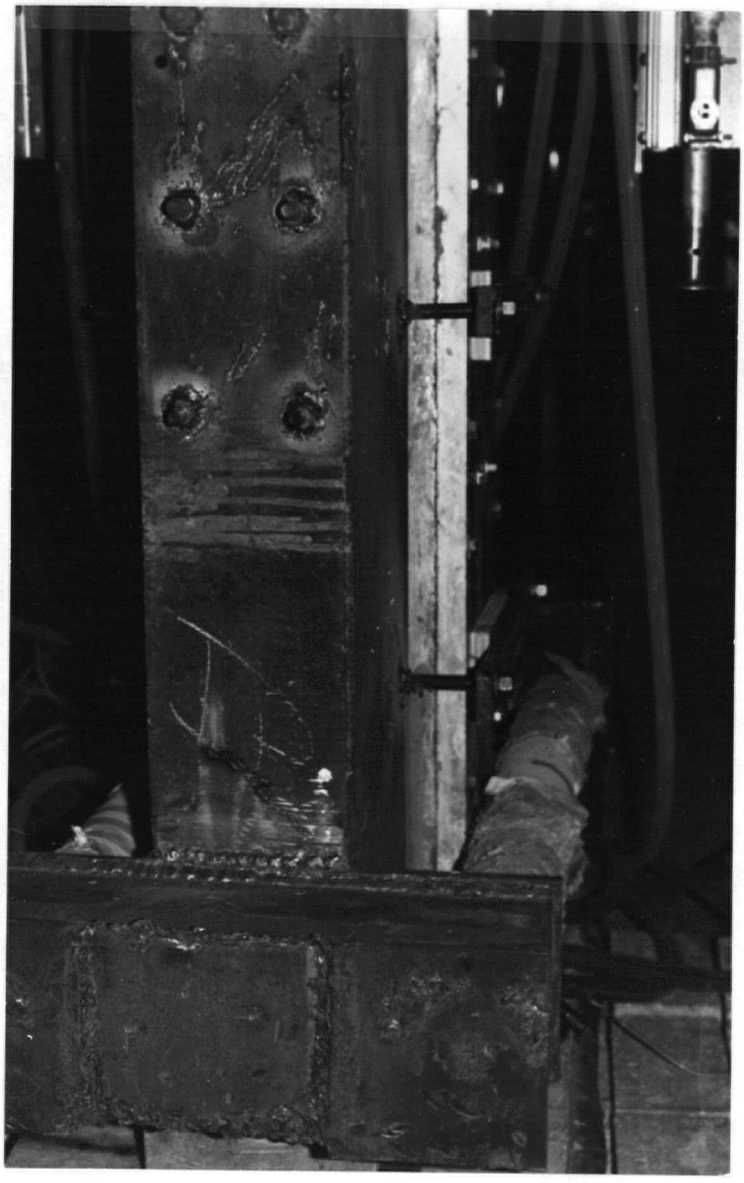

Figure 22 - Inferior I-beam Placement

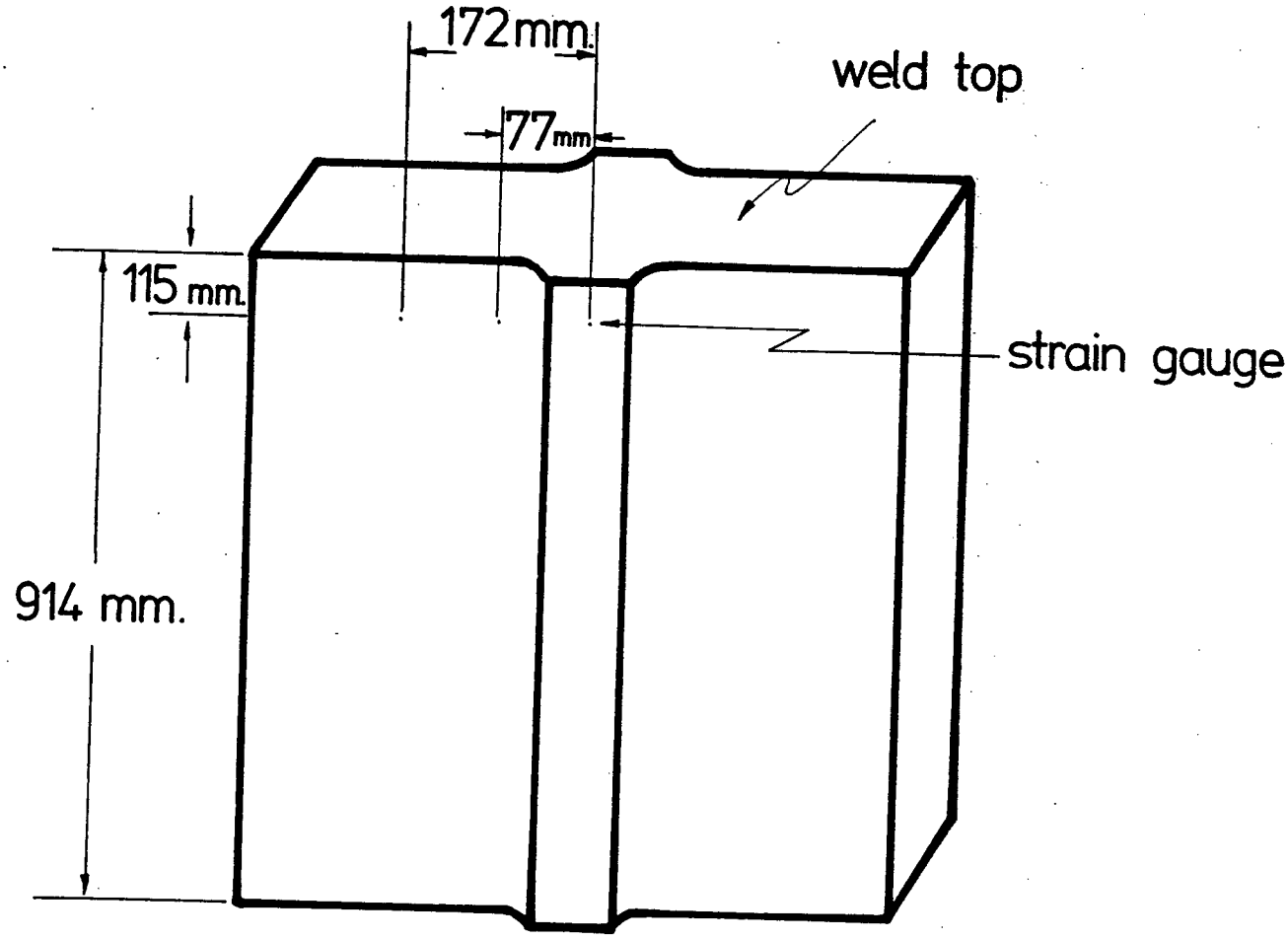

Figure 23 - Strain-gauge Set-up

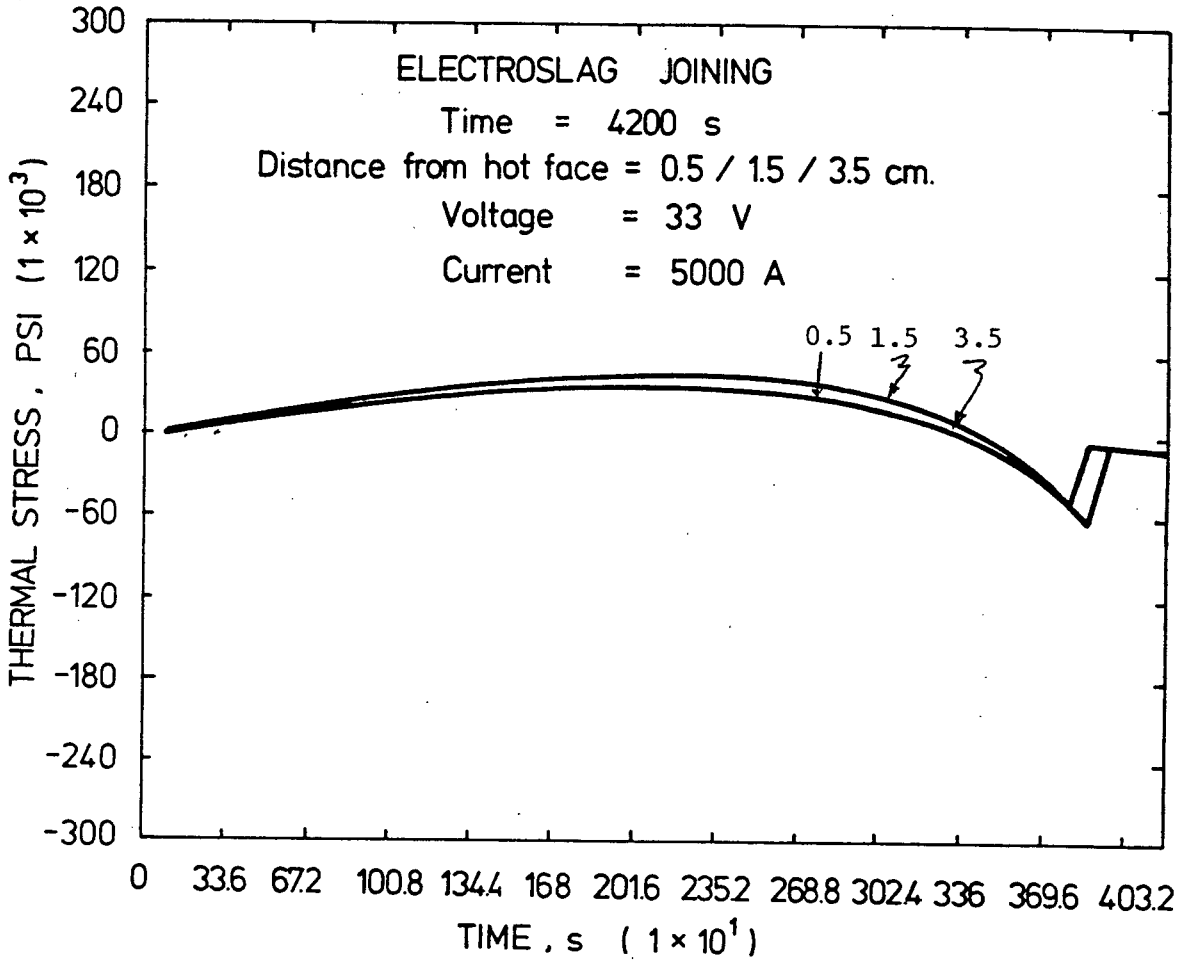

Figure 24 - Thermal Stress Curve

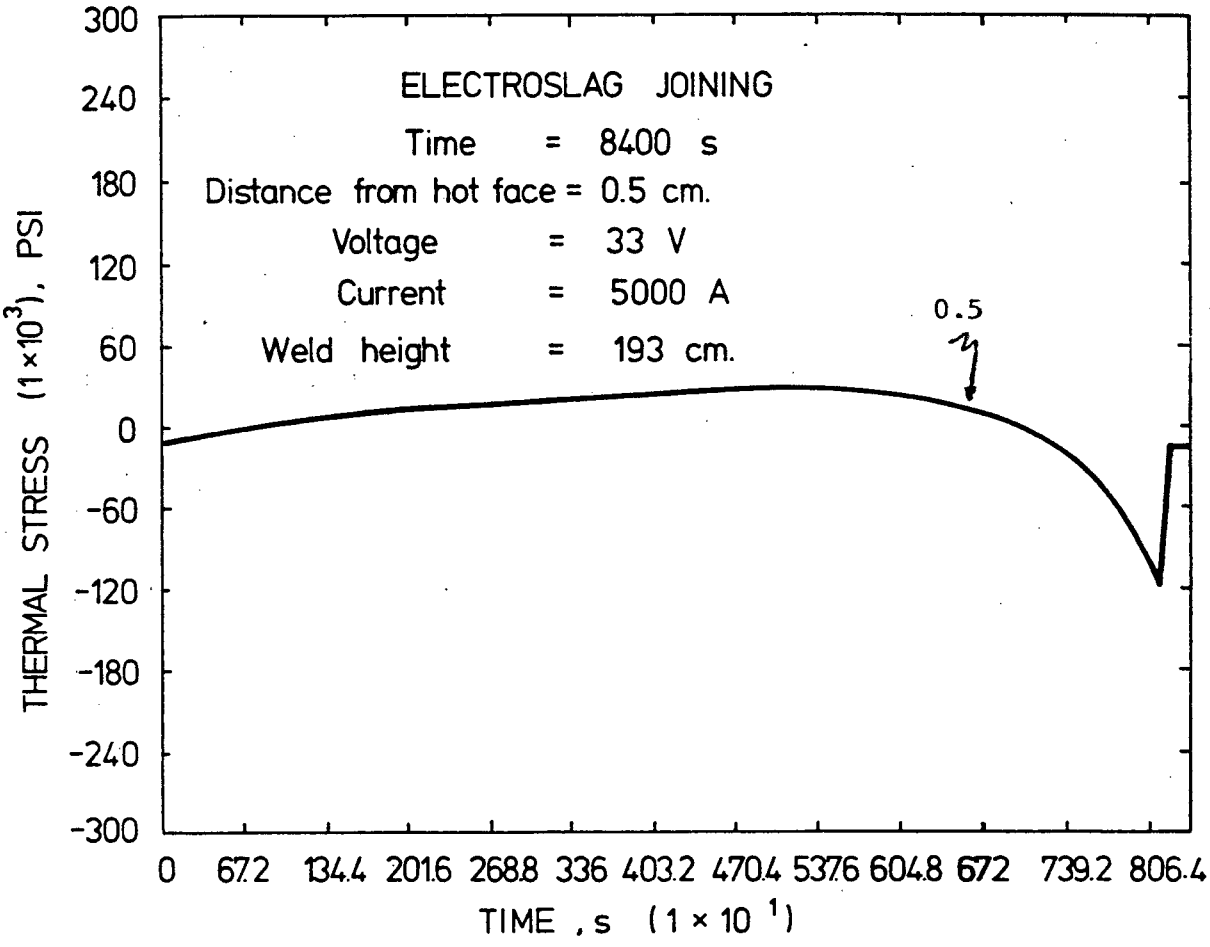

Figure 25 - Thermal Stress Curve

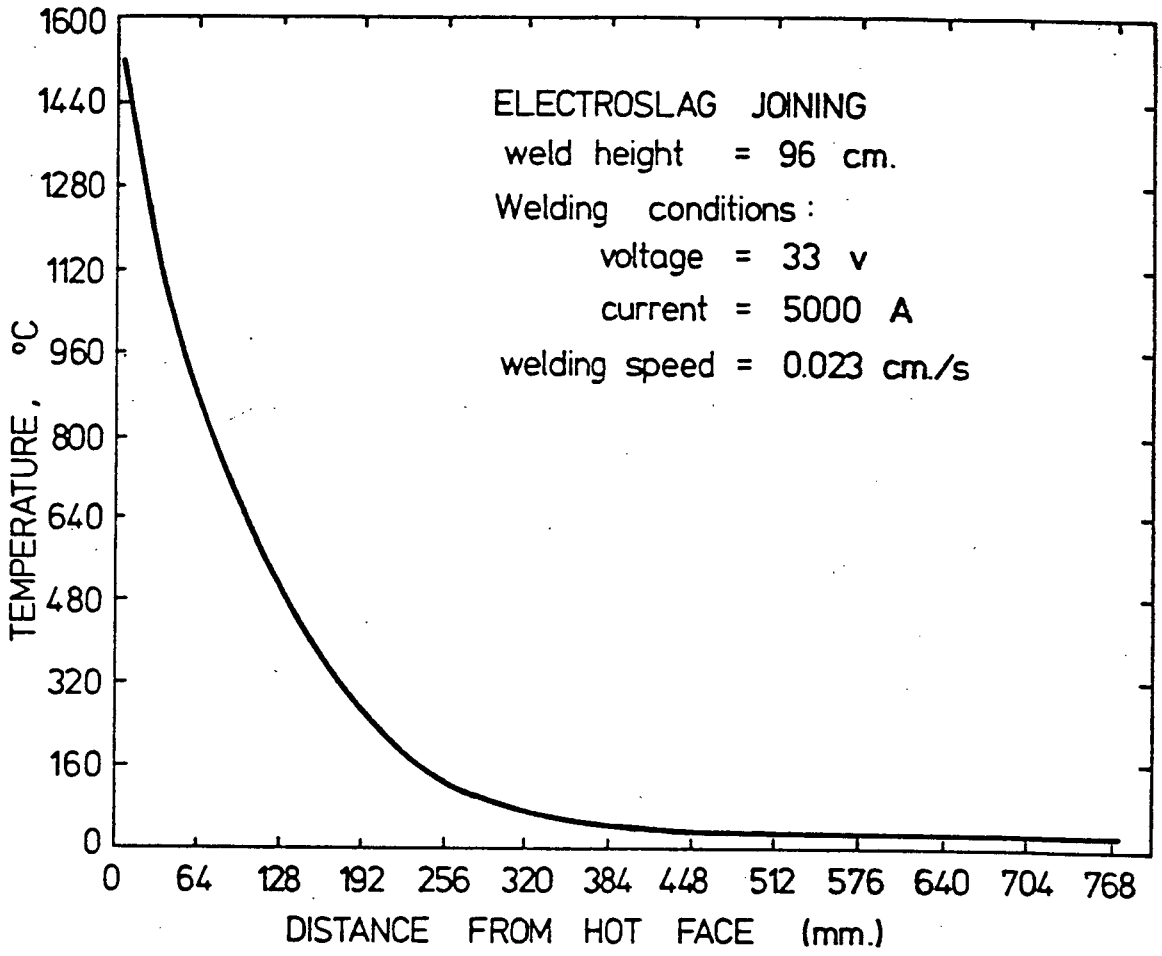

Figure 26 - ESJ Thermal Gradient

APPENDIX A - BOUNDARY CONDITIONS

BOUNDARY I(i=1,j=1)

i) If element I contacts the heat source:

1st $\frac{\Delta t}{2}$ $\qquad T^{*}_{1,1} = T_{MP}$

2nd $\frac{\Delta t}{2}$ $\qquad T^{n+1}_{1,1} = T_{MP}$

ii) If element I does not contact the heat source, the following equation can be obtained by applying a heat balance:

1st $\frac{\Delta t}{2}$

$$\Delta y \frac{\Delta x}{2} C\rho \frac{(T^{*}_{1,1} - T^{n}_{1,1})}{\frac{\Delta t}{2}} = \frac{k \Delta y 1}{x}(T^{*}_{2,1} - T^{*}_{1,1}) + \frac{\frac{k\Delta x}{2}}{\Delta y_1 + \frac{\Delta y_2}{2}}(T^{n}_{1,2} - T^{n}_{1,1})$$

or

$$\left(\frac{2}{\Delta t} + \frac{2}{\Delta x^2}\right) T^{*}_{1,1} - \frac{2\alpha}{\Delta x^2} T^{*}_{2,1} = \frac{2}{\Delta t} T^{n}_{1,1} + \frac{\alpha}{\Delta y_1 (\Delta y_1 + \frac{\Delta y_2}{2})}(T^{n}_{1,2} - T^{n}_{1,1})$$

2nd $\frac{\Delta t}{2}$

$$\Delta y_1 \frac{\Delta x}{2} C\rho \frac{(T^{n+1}_{1,1} - T^{*}_{1,1})}{\frac{\Delta t}{2}} = \frac{k \Delta y_1}{\Delta x}(T^{*}_{2,1} - T^{*}_{1,1}) + \frac{\frac{k\Delta x}{2}}{\Delta y_1 + \frac{\Delta y 2}{2}}(T^{n+1}_{1,2} - T^{n+1}_{1,1})$$

or

$$\left(\frac{2}{\Delta t} + \frac{\alpha}{\Delta y_1 (\Delta y_1 + \frac{\Delta y_2}{2})}\right) T^{n+1}_{1,1} - \frac{\alpha\, T^{n+1}_{1,2}}{\Delta y_1 (\Delta y_1 + \frac{\Delta y_2}{2})} = \frac{2}{\Delta t} T^{*}_{1,1} + \frac{2\alpha}{\Delta x^2}(T^{*}_{2,1} - T^{*}_{1,1})$$

BOUNDARY II(i=2-IM-1,j=1)

i) If element II contacts the heat source:

1st $\frac{\Delta t}{2}$ $\qquad T^{*}_{i,1} = T_{MP}$

2nd $\frac{\Delta t}{2}$ $\qquad T^{n+1}_{i,1} = T_{MP}$

ii) If element II does not contact the heat source, the following equation can be obtained by applying a heat balance:

1st $\frac{\Delta t}{2}$

$$\Delta y_1 \Delta x \rho Cp \frac{(T^{*}_{i,1} - T^{n}_{i,1})}{\frac{\Delta t}{2}} = \frac{k\Delta y_1}{\Delta x}(T^{*}_{i+1,1} + T^{*}_{i-1,1} - 2T^{*}_{i,1}) + \frac{k\Delta x}{\Delta y_1 + \frac{\Delta y_2}{2}}(T^{n}_{1,2} - T^{n}_{i,1}) \quad \text{or}$$

$$-\frac{\alpha}{\Delta x^2} T^{*}_{i-1,1} + \left(\frac{2}{\Delta t} + \frac{2}{\Delta x^2}\right) T^{*}_{i,1} - \frac{\alpha}{\Delta x^2} T^{*}_{i+1,1} = \frac{2}{\Delta t} T^{n}_{i,1} + \frac{\alpha}{\Delta y_1 (\Delta y_1 + \frac{\Delta y_2}{2})}(T^{n}_{i,2} - T^{n}_{i,1})$$

2nd $\frac{\Delta t}{2}$

$$\Delta y_1 \Delta x \rho Cp \frac{(T^{n+1}_{i,1} - T^{*}_{i,1})}{\frac{\Delta t}{2}} = \frac{k\Delta y_1}{\Delta x}(T^{*}_{i+1,1} + T^{*}_{i-1,1} - 2T^{*}_{i,j}) + \frac{k\,\Delta x}{\Delta y_1 + \frac{\Delta y_2}{2}}(T^{n+1}_{1,2} - T^{n+1}_{i,1})$$

or

$$\left(\frac{2}{\Delta t} + \frac{\alpha}{\Delta y_1 (\Delta y_1 + \frac{\Delta y_2}{2})}\right) T^{n+1}_{i,1} - \frac{\alpha}{\Delta y_1 (\Delta y_1 + \frac{\Delta y_2}{2})} T^{n+1}_{i,2} = \frac{2}{\Delta t} T^{*}_{i,1} + \frac{\alpha}{\Delta x^2}(T^{*}_{i+1,1} + T^{*}_{i-1,1} - 2T^{*}_{i,1})$$

BOUNDARY III(i=IM,j=1)

i) If element III contacts the heat source:

1st $\frac{\Delta t}{2}$ $\qquad T^{*}_{IM,1} = T_{MP}$

2nd $\frac{\Delta t}{2}$ $\qquad T^{n+1}_{IM,1} = T_{MP}$

ii) If element III does not contact the heat source, the following equation can be obtained by applying a heat balance:

1st $\frac{\Delta t}{2}$

$$\Delta y_1 \frac{\Delta x}{2}\rho Cp\left(\frac{T^{*}_{IM,1} - T^{n}_{IM,1}}{\frac{\Delta t}{2}}\right) = -\frac{k\Delta y_1}{\Delta x}(T^{*}_{IM,1} - T^{*}_{IM,1}) + \frac{\frac{k\Delta x}{2}(T^{n}_{IM,2} - T^{*}_{IM,1})}{(\Delta y_1 + \frac{\Delta y_2}{2})} \quad \text{or}$$

$$-\frac{2\alpha}{\Delta x^2}T^{*}_{IM-1,1} + \left(\frac{2}{\Delta t} + \frac{2\alpha}{\Delta x^2}\right)T^{*}_{IM,1} = \frac{2}{\Delta t}T^{n}_{IM,1} + \frac{\alpha}{\Delta y_1(\Delta y_1 + \frac{\Delta y_2}{2})}(T^{n}_{IM,2} - T^{n}_{IM,1})$$

2nd $\frac{\Delta t}{2}$

$$\frac{\Delta x}{2}\rho Cp\left(\frac{T^{n+1}_{IM,1} - T^{*}_{IM,1}}{\frac{\Delta t}{2}}\right) = -\frac{k\Delta y_1}{\Delta x}(T^{*}_{IM,1} - T^{*}_{IM-1,1}) + \frac{\frac{k\Delta x}{2}(T^{n+1}_{IM,2} - T^{n+1}_{IM,1})}{\Delta y_1 + \frac{\Delta y_2}{2}} \quad \text{or}$$

$$\left(\frac{2}{\Delta t} + \frac{\alpha}{\Delta y_1(\Delta y_1 + \frac{\Delta y_2}{2})}\right)T^{n+1}_{IM,1} - \frac{\alpha}{\Delta y_1(\Delta y_1 + \frac{\Delta y_2}{2})}T^{n+1}_{IM,2} = \frac{2}{\Delta t}T^{*}_{IM,1} - \frac{2\alpha}{\Delta x^2}(T^{*}_{IM,1} - T^{*}_{IM-1,1})$$

BOUNDARY IV(i=1,j=2-IN-1)

$$1st\ \frac{\Delta t}{2}\qquad \frac{\Delta x\Delta y_j}{2}\rho Cp\left(\frac{T^*_{1,j}-T^n_{1,j}}{\frac{\Delta t}{2}}\right)=\frac{k\Delta y_j(T^*_{2,j}-T^*_{1,j})}{\Delta x}$$

$$+\frac{\frac{k\Delta x}{2}(T^n_{1,j+1}-T^n_{1,j})}{\frac{\Delta y_j+\Delta y_{j+1}}{2}}-\frac{\frac{k\Delta x}{2}(T^n_{1,j}-T^n_{1,j-1})}{\frac{\Delta y_j+\Delta y_{j-1}}{2}}$$

or

$$\left(\frac{2}{\Delta t}+\frac{2}{\Delta x^2}\right)T^*_{1,j}-\frac{2\alpha}{\Delta x^2}T^*_{2,j}=\frac{2}{\Delta t}T^n_{1,j}+\frac{2\alpha(T^n_{1,j+1}-T^n_{1,j})}{\Delta y_j(\Delta y_j+\Delta y_{j+1})}-\frac{2\alpha(T^n_{1,j}-T^n_{1,j-1})}{\Delta y_j(\Delta y_j+\Delta y_{j-1})}$$

$$2nd\ \frac{\Delta t}{2}\qquad \frac{\Delta x\Delta y_j}{2}\rho Cp\left(\frac{T^{n+1}_{1,j}-T^*_{1,j}}{\frac{\Delta t}{2}}\right)=\frac{k\Delta y_j(T^*_{2,j}-T^*_{1,j})}{\Delta x}+$$

$$+\frac{\frac{k\Delta x}{2}(T^{n+1}_{1,j+1}-T^{n+1}_{1,j})}{\frac{\Delta y_j+\Delta y_{j+1}}{2}}-\frac{\frac{k\Delta x}{2}(T^{n+1}_{1,j}-T^{n+1}_{1,j-1})}{\frac{\Delta y_j+\Delta y_{j-1}}{2}}$$

or

$$\frac{-2\alpha}{\Delta y_j(\Delta y_j+\Delta y_{j-1})}T^{n+1}_{1,j-1}+\left(\frac{2}{\Delta t}+\frac{2\alpha}{\Delta y_j(\Delta y_j+\Delta y_{j+1})}+\frac{2\alpha}{\Delta y_j(\Delta y_j+\Delta y_{j-1})}\right)T^{n+1}_{1,j}+$$

$$-\frac{2\alpha}{\Delta y_j(\Delta y_j+\Delta y_{j+1})}T^{n+1}_{1,j+1}=\frac{2}{\Delta t}T^*_{1,j}+\frac{2\alpha}{\Delta x^2}(T^*_{2,j}-T^*_{1,j})$$

BOUNDARY V(i=IM,j=IN-1)

$$\text{1st } \frac{\Delta t}{2}\ \frac{\Delta x \Delta y_j}{2}\rho Cp\left(\frac{T^*_{IM,j} - T^*_{IM,j}}{\frac{\Delta t}{2}}\right) = \frac{-K\Delta y_j}{\Delta x}\left(T^*_{IM,j} - T^*_{IM-1,j}\right) + \frac{K\frac{\Delta x}{2}\left(T^n_{IM,j+1} - T^n_{IM,j}\right)}{\frac{\Delta y_j + \Delta y_{j+1}}{2}} - \frac{K\frac{\Delta x}{2}\left(T^n_{IM,j} - T^n_{IM,j-1}\right)}{\frac{\Delta y_j + \Delta y_{j-1}}{2}}$$

or

$$-\frac{2\alpha}{\Delta x^2}T^*_{IM-1,j} + \left(\frac{2}{\Delta t} + \frac{2\alpha}{\Delta x^2}\right)T^*_{IM,j} = \frac{2}{\Delta t}T^n_{IM,J} + \frac{2\alpha\left(T^n_{IM,j=1} - T^n_{IM,j}\right)}{\Delta y_j\left(\Delta y_j + \Delta y_{j+1}\right)} - \frac{2\alpha\left(T^n_{IM,j} - T^n_{IM,j-1}\right)}{\Delta y_j\left(\Delta y_j + \Delta y_{j-1}\right)}$$

$$\text{2nd } \frac{\Delta t}{2}\ \frac{\Delta x \Delta y_j}{2}\rho\, Cp\left(\frac{T^{n+1}_{IM,j} - T^*_{IM,j}}{\frac{\Delta t}{2}}\right) = \frac{-K\Delta y_j}{\Delta x}\left(T^*_{IM,j} - T^*_{IM-1,j}\right) + \frac{k\frac{\Delta x}{2}\left(T^{n+1}_{IM,j+1} - T^{n+1}_{IM,j}\right)}{\frac{\Delta y_j + \Delta y_{j+1}}{2}} - \frac{k\frac{\Delta x}{2}\left(T^{n+1}_{IM,j} - T^{n+1}_{IM,j-1}\right)}{\frac{\Delta y_j + \Delta y_{j-1}}{2}}$$

or

$$\frac{-2\alpha}{\Delta y_j\left(\Delta y_j + \Delta y_{j-1}\right)}T^{n+1}_{IM,j-1} + \left(\frac{2}{\Delta t} + \frac{2\alpha}{\Delta y_j\left(\Delta y_j + \Delta y_{j+1}\right)} + \frac{2\alpha}{y_j\left(\Delta y_j + \Delta y_{j-1}\right)}\right)T^{n+1}_{IM,j} +$$

$$-\frac{2\alpha}{\Delta y_j\left(\Delta y_j + \Delta y_{j+1}\right)}T^{n+1}_{IM,j+1} = \frac{2}{\Delta t}T^*_{IM,j} - \frac{2\alpha}{\Delta x^2}\left(T^*_{IM,j} - T^*_{IM-1,j}\right)$$

BOUNDARY VI(i=1,j=IN)

$$\text{1st } \frac{\Delta t}{} \quad \frac{\Delta x \Delta y_{IN} \rho Cp}{2}\left(\frac{T^{*}_{1,IN} - T^{n}_{1,IN}}{\frac{\Delta t}{2}}\right) = \frac{K \Delta y_{IN}}{\Delta x}\left(T^{*}_{2,IN} - T^{*}_{1,IN}\right) +$$

$$- \frac{K \frac{\Delta x}{2}\left(T^{n}_{1,IN} - T^{n}_{1,IN-1}\right)}{\Delta y_{IN} + \frac{\Delta y_{IN-1}}{2}}$$

or

$$\left(\frac{2}{\Delta t} + \frac{2\alpha}{\Delta x^{2}}\right) T^{*}_{1,IN} - \frac{2\alpha}{\Delta x^{2}} T^{*}_{2,IN} = \frac{2}{\Delta t} T^{n}_{1,IN} - \frac{\alpha\left(T^{n}_{1,IN} - T^{n}_{1,IN-1}\right)}{\Delta y_{IN}\left(\Delta y_{IN} + \frac{\Delta y_{IN-1}}{2}\right)}$$

$$\text{2nd } \frac{\Delta t}{2} \quad \frac{\Delta x}{2} \quad \Delta Y_{IN} \rho Cp \left(\frac{T^{n+1}_{1,IN} - 1,IN}{\frac{\Delta t}{2}}\right) = \frac{K \Delta y_{IN}}{\Delta k}\left(T^{*}_{2,IN} - T^{*}_{1,IN}\right) +$$

$$- \frac{K \frac{\Delta x}{2}\left(T^{n+1}_{1,IN} - T^{n+1}_{1,IN-1}\right)}{\Delta y_{IN} + \frac{\Delta y_{IN-1}}{2}}$$

or

$$\frac{- \alpha}{\Delta y_{IN}\left(\Delta y_{IN} + \frac{\Delta y_{IN-1}}{2}\right)} T^{n+1}_{1,IN-1} + \frac{2}{\Delta t} + \frac{\alpha}{\Delta y_{IN}\left(\Delta y_{IN} + \frac{\Delta y_{IN-1}}{2}\right)} T^{n+1}_{1,IN} =$$

$$\frac{2}{\Delta t} T^{*}_{1,IN} + \frac{2\alpha}{\Delta x^{2}}\left(T^{*}_{2,IN} - T^{*}_{1,IN}\right)$$

·BOUNDARY VII (i=2-IM-1,j=IN)

$$1st\ \frac{\Delta t}{2}\ \Delta x\Delta y_{IN}\rho Cp\ \frac{(T^*_{i,IN}-T^*_{i,IN})}{\frac{\Delta t}{2}} =$$

$$\frac{K\Delta y_{IN}}{t}(T^*_{i+1,IN}+T^*_{i-1,IN}-2T^*_{1,IN})-\frac{K\Delta x(T^n_{i,IN}-T^n_{i,IN-1})}{\Delta y_{IN}+\frac{\Delta y_{IN-1}}{2}}$$

or

$$\frac{-\alpha}{\Delta x^2}T^*_{i-1,IN}+\left(\frac{2}{\Delta t}+\frac{2\alpha}{\Delta x^2}\right)T^*_{i,IN}-\frac{\alpha}{\Delta x^2}T^*_{i+1,IN}=\frac{2}{\Delta t}T^n_{1,IN}+$$

$$-\frac{\alpha(T^n_{i,IN}-T^n_{i,IN-1})}{\Delta y_{IN}(\Delta y_{IN}+\frac{\Delta y_{IN-1}}{2})}$$

$$2nd\ \frac{\Delta t}{2}\ \Delta x\Delta y_{IN}\rho Cp\left(\frac{T^{n+1}_{i,IN}-T^*_{1,IN}}{\frac{\Delta t}{2}}\right)=-\frac{K\Delta x(T^{n+1}_{i,IN}-T^{n+1}_{i,IN-1})}{\Delta y_{IN}+\frac{\Delta y_{IN-1}}{2}}$$

$$+\frac{K\Delta y_{IN}}{\Delta x}(T^*_{i+1,IN}+T^*_{i-1,IN}-2T^*_{i,IN})$$

or

$$\frac{-\alpha}{\Delta y_{IN}(\Delta y_{IN}+\frac{\Delta y_{IN-1}}{2})}T^{n+1}_{i,IN-1}+\left(\frac{2}{\Delta t}+\frac{\alpha}{\Delta y_{IN}(\Delta y_{IN}+\frac{\Delta y_{IN-1}}{2})}\right)T^{n+1}_{i,IN}=$$

$$\frac{2}{\Delta t}T^*_{i,IN}+\frac{\alpha}{\Delta x^2}(T^*_{i,IN}+T^*_{i-I,IN}-2T^*_{i,IN})$$

BOUNDARY VIII (i=IM, j=IN)

$$1st\ \frac{\Delta t}{2}\ \frac{\Delta x \Delta y_{IN} \rho Cp}{2}\ \frac{(T^{*}_{IM,IN} - T^{n}_{IM,IN})}{\frac{t}{2}} =$$

$$- \frac{K\Delta y_{IN}}{\Delta x}(T^{*}_{IM,IN} - T^{*}_{IM-1,IN}) - \frac{K\frac{\Delta x}{2}(T^{n}_{IM,IN} - T^{n}_{IM,IN-1})}{\Delta y_{IN} + \frac{\Delta y_{IN-1}}{2}}$$

Or

$$\frac{-2\alpha}{\Delta x^2} T^{*}_{IM-1,IN} + \left(\frac{2}{\Delta t} + \frac{2\alpha}{\Delta x^2}\right) T^{*}_{IM,IN} = \frac{2}{\Delta t} T^{n}_{IM,IN} +$$

$$- \frac{\alpha (T^{n}_{IM,IN} - T^{n}_{IM,IN-1})}{\Delta y_{IN}(\Delta y_{IN} + \frac{\Delta y_{IN-1}}{2})}$$

$$2nd\ \frac{\Delta t}{2}\ \frac{\Delta x \Delta y_{IN} \rho Cp}{2}\ \frac{(T^{n+1}_{IM,IN} - T^{*}_{IM,IN})}{\frac{\Delta t}{2}} =$$

$$- \frac{K\Delta Y_{IN}}{\Delta x}(T^{*}_{IM,IN} - T^{*}_{IM-1,IN}) - \frac{K\frac{\Delta x}{2}(T^{n+1}_{IM,IN} - T^{n+1}_{IM,IN-1})}{\Delta y_{IN} + \frac{\Delta y_{IN-1}}{2}}$$

or

$$\frac{-\alpha}{\Delta y_{IN}(\Delta y_{IN} + \frac{\Delta y_{IN-1}}{2})} T^{n+1}_{IN,In-1} + \left(\frac{2}{\Delta t} + \frac{\alpha}{\Delta y_{IN}\left(\frac{\Delta y_{IN} + \Delta y_{IN-1}}{2}\right)}\right) T^{n+1}_{IM,IN} =$$

$$\frac{2}{\Delta t} T^{*}_{IM,IN} - \frac{2\alpha}{\Delta x^2}(T^{*}_{IM,IN} - T^{*}_{IM-1,IN})$$

APPENDIX B - COMPUTER PROGRAM SAMPLE

```
C      CALCULATION OF THERMAL STRESSES IN HEAVY SECTION
C      ELECTROSLAG JOINING
C
C
C
C      PAULO SILVEIRA IVO
C
C
C
C      MAIN PROGRAM
C
       DIMENSION T(100,100),TS(100,100),TB(100,100),DY(100),ID(100)
       CALL DINPUT(DY,DX,TMP,TBO,DT,CP,RO,AK,DPH,PRNT,TLAST,IM,
      *IN,XI,VO,TH,F,G,SE,SWG,AL,FR,CPW,DELT,ROW,HEB)
C
       CALL INITL(T,TS,TB,TBO,DPH,DX,ID,IM,IN,PRNT,PRNTO)
C
       CALL VEL(V,F,XI,VO,Q1,IM,DT,DX,TH,T,DY,DPH,AK,IN,TBO,TMP,ID)
C
       TIME=0.0
     1 TIME=TIME+DT
C
       CALL HSPOS(DPH,V,TIME,DX,ID,IM)
C
       CALL CONST(DT,DX,CP,RO,AK,ALPHA,A1,A2,A3)
C
       CALL FSTS(TB,TS,DY,DX,DT,ALPHA,IN,IM,TMP,ID,A1,A2,A3)
C
       CALL SNDS(TS,T,DY,DX,DT,ALPHA,IN,IM,TMP,ID,A1,A2,A3)
C
       CALL HEAT(XI,VO,AK,CP,RO,DX,DPH,TH,T,TMP,ID,G,F,IM,IN,TBO,DY,
      *DT,V,TIME,SE,SWG,AL,FR,CPW,DELT,ROW,HEB)
C
       CALL PRINT(T,TIME,IN,IM,IP,PRNT,PRNTO,TLAST,ID)
C
       IF(IP.EQ.1) GO TO 2
       DO 10 I=1,IM
       DO 20 J=1,IN
       TB(I,J)=T(I,J)
    20 CONTINUE
    10 CONTINUE
       GO TO 1
     2 CALL STRESS(T,TT,TTT,IT,IM,IN,ALFA,H)
       STOP
       END
C
C      READ DATA AND PRINT HEADINGS
C
       SUBROUTINE DINPUT(DY,DX,TMP,TBO,DT,CP,RO,AK,DPH,PRNT,TLAST,IM,
      *IN,XI,VO,TH,F,G,SE,SWG,AL,FR,CPW,DELT,ROW,HEB)
C
       DIMENSION DY(100)
       READ(5,100) TMP,TBO,DT,CP,RO,AK,DX,F,DPH,PRNT,TLAST
   100 FORMAT(F6.1,9F6.3,F10.0)
       READ(5,110) IM,IN
   110 FORMAT(2I3)
```

```
      READ(5,120) DY(1),DY(2),DY(3),DY(4),DY(5),DY(6),DY(7)
  120 FORMAT(7F5.0)
      DO 10 I=8,IN
      DY(I)=DY(7)
   10 CONTINUE
      READ(5,130) G,TH,XI,VO,SE,SWG,AL
  130 FORMAT(7F6.1)
      READ(5,140) FR,CPW,DELT,ROW,HEB
  140 FORMAT(4F6.3,F7.4)
      WRITE(6,200)
  200 FORMAT(1H ,///,5X,' ESW THERMAL PROFILE ',3X,
     *'PAULO  S.  IVO',/,6X,19('*'),///)
      WRITE(6,210) TMP,TBO,DT,CP,RO,AK,DX,F,DPH,PRNT,TLAST
  210 FORMAT(1H ,1X,'TMP=',F6.1,1X,'(Deg C)',/,2X,'INITIAL TEMP=',
     *F6.1,1X,'(Deg C)',/,2X,
     *'TIME STEP=',F6.1,1X,'(s)',/,2X,'SPECIFIC HEAT=',F6.4,1X,
     *'(cal/g.C)'
     *,/,2X,'DENSITY=',F6.3,1X,'(g/cm**3)',/,2X,
     *'CONDUCTIVITY=',F6.4,1X,'(cal/cm.s.C)',/,2X,'DX=',
     *F6.1,1X,'(cm)',/,2X,'HEAT FACTOR=',F6.3,1X,
     */,2X,'HEAT SOURCE DEPTH=',F6.3,1X,'(cm)',/,
     *2X,'PRINT CYCLE=',F7.1,1X,'(s)',/,2X,'END OF CALCULATION='
     *,F10.1,1X,'(s)')
      WRITE(6,220) (DY(I),I=1,IN)
  220 FORMAT(1H ,1X,'DY=',10F6.1)
      WRITE(6,230) IM,IN
  230 FORMAT(1H ,1X,'NUMBER OF DIVISIONS IN X-DIRECTION =',I3,//,
     *2X,'NUMBER OF DIVISIONS IN Y-DIRECTION =',I3)
      WRITE(6,240) G,TH,XI,VO,SE,SWG,AL
  240 FORMAT(1H ,///,2X,'WELDING PARAMETERS',///,2X,
     *'WELD GAP=',F5.1,1X,'cm',2X,'THICKNESS=',F5.1,1X,'cm',//
     *2X,'CURRENT=',F7.1,1X,'A',2X,'VOLTAGE=',F5.1,1X,'V',//,
     *2X,'ELECTRODE SURFACE AREA=',F5.1,1X,'(cm**2)',2X,
     *'WELD GAP AREA=',F6.1,1X,'(cm**2)',2X,//,2X,'LATENT HEAT=',
     *F5.1,1X,'(cal/g)',//)
      WRITE(6,250) FR,CPW,DELT,ROW,HEB
  250 FORMAT(1H ,1X,'WATER FLOW RATE=',F6.1,1X,'(cm**3/s)',
     */,2X,'WATER SPECIFIC HEAT=',F6.1,1X,'(cal/g.C)',/,
     *2X,'TEMP. DIFF. IN MOULD=',F6.1,1X,'(C)',/,2X,
     *'WATER DENSITY=',F6.1,1X,'(g/cm**3)',/,2X,
     *'HEAT EFF. TO THE BLOCKS=',F7.4,1X,/)
      RETURN
      END
C
C
C
C
C
C
      SUBROUTINE INITL(T,TS,TB,TBO,DPH,DX,ID,IM,IN,PRNT,PRNTO)
C
      DIMENSION T(100,100),TS(100,100),TB(100,100),ID(100)
      DO 10 I=1,IM
      DO 20 J=1,IN
      T(I,J)=TBO
      TS(I,J)=TBO
      TB(I,J)=TBO
   20 CONTINUE
   10 CONTINUE
      NO=IFIX(DPH/DX+0.49)+1
```

```
      DO 30 I=1,NO
   30 ID(I)=1
      NP=NO+1
      DO 40 I=NP,IM
   40 ID(I)=0
      PRNTO=PRNT
      RETURN
      END
C
C
C     CALCULATION OF THE WELDING SPEED
C
C
C
      SUBROUTINE VEL(V,F,XI,VO,Q1,IM,DT,DX,TH,T,DY,DPH,AK,IN,TBO,
     *TMP,ID)
      DIMENSION ID(100),T(100,100),DY(100)
      CALL HEAT1(AK,DX,TH,T,DY,ID,Q1,IM,DPH,DT,IN,TBO,TMP)
      FACTOR=0.24*0.95*0.35*XI*VO/(.023*Q1)
      V=((.35*XI*VO*0.24*.95)/(FACTOR*Q1))
      WRITE(6,888) V,FACTOR
  888 FORMAT(1H ,/,'WELDING VELOCITY=',F6.3,2X,'(cm/s)',F7.2,/)
      RETURN
      END
C
C     DECISION ON WHETHER THE HEAT SOURCE IS CONTACTING THE BLOCK
C
      SUBROUTINE HSPOS(DPH,V,TIME,DX,ID,IM)
C
      DIMENSION ID(100)
      NO=IFIX(V*TIME/DX+0.51)+1
      NS=IFIX((DPH+V*TIME)/DX+0.49)+1
      NN=NO-1
      IF(NO-1) 1,1,2
    2 DO 10 I=1,NN
      ID(I)=0
   10 CONTINUE
    1 DO 20 I=NO,NS
      ID(I)=1
   20 CONTINUE
      NNS=NS+1
      DO 30 I=NNS,IM
      ID(I)=0
   30 CONTINUE
      RETURN
      END
C
C
C
      SUBROUTINE CONST(DT,DX,CP,RO,AK,ALPHA,A1,A2,A3)
C
      ALPHA=AK/(CP*RO)
      A1=2.0*(1.0/DT+ALPHA/(DX**2))
      A2=2.0*ALPHA/(DX**2)
      A3=2.0/DT
      RETURN
      END
C
C
C
```

```
C
C     CALCULATION OF THE FIRST HALF-TIME STEP
C
C
C
C
      SUBROUTINE FSTS(TB,TS,DY,DX,DT,ALPHA,IN,IM,TMP,ID,A1,A2,A3)
C
      DIMENSION TB(100,100),TS(100,100),DY(100),ID(100)
      DIMENSION A(100),B(100),C(100),D(100),TPRIME(100)
C
      IF(ID(1)-1) 1,2,2
    2 CALL SOURCE(A(1),B(1),C(1),D(1),TMP)
      GO TO 3
    1 A(1)=0.0
      B(1)=A1
      C(1)=-A2
      D(1)=A3*TB(1,1)+ALPHA/(DY(1)*(DY(1)+0.5*DY(2)))
     **(TB(1,2)-TB(1,1))
    3 CONTINUE
      IJ=IM-1
      IK=IN-1
      DO 10 I=2,IJ
      IF(ID(I)-1) 4,5,5
    5 CALL SOURCE(A(I),B(I),C(I),D(I),TMP)
      GO TO 10
C
    4 A(I)=-0.5*A2
      B(I)=A1
      C(I)=-0.5*A2
C
      D(I)=A3*TB(I,1)+(ALPHA/(DY(1)*(DY(1)+0.5*DY(2)))
     **(TB(I,2)-TB(I,1)))
C
   10 CONTINUE
C
      IF(ID(IM)-1) 6,7,7
    7 CALL SOURCE(A(IM),B(IM),C(IM),D(IM),TMP)
      GO TO 8
C
    6 A(IM)=-A2
      B(IM)=A1
      C(IM)=0.0
C
      D(IM)=A3*TB(IM,1)+(ALPHA/(DY(1)*(DY(1)+0.5*DY(2)))
     **(TB(IM,2)-TB(IM,1)))
C
    8 CALL TRIDAG(1,IM,A,B,C,D,TPRIME)
C
      DO 15 I=1,IM
   15 TS(I,1)=TPRIME(I)
      DO 20 J=2,IK
C
      A(1)=0.0
      B(1)=A1
      C(1)=-A2
      D(1)=A3*TB(1,J)+(2.0*ALPHA/(DY(J)*(DY(J)+DY(J+1))))
     **(TB(1,J+1)-TB(1,J))-(2.0*ALPHA/(DY(J)*(DY(J)
     *+DY(J-1))))*(TB(1,J)-TB(1,J-1))
C
```

```
C
      DO 25 I=2,IJ
C
      A(I)=-0.5*A2
      B(I)=A1
      C(I)=A(I)
C
      D(I)=A3*TB(I,J)+(2.0*ALPHA*(TB(I,J+1)-TB(I,J))/
     *(DY(J)*(DY(J)+DY(J+1))))
     *-(2.0*ALPHA*(TB(I,J)-TB(I,J-1))/(DY(J)*(DY(J)+DY(J-1))))
C
   25 CONTINUE
C
C
      A(IM)=-A2
      B(IM)=A1
      C(IM)=0.0
C
      D(IM)=A3*TB(IM,J)+(2.0*ALPHA*(TB(IM,J+1)-TB(IM,J))
     */(DY(J)*(DY(J)+DY(J+1))))-(2.0*ALPHA*(TB(IM,J)
     *-TB(IM,J-1))/(DY(J)*(DY(J)+DY(J-1))))
C
      CALL TRIDAG(1,IM,A,B,C,D,TPRIME)
C
      DO 30 I=1,IM
   30 TS(I,J)=TPRIME(I)
   20 CONTINUE
C
      A(1)=0.0
      B(1)=A1
      C(1)=-A2
C
      D(1)=A3*TB(1,IN)-(ALPHA*(TB(1,IN)-TB(1,IN-1))
     */(DY(IN)*(DY(IN)+0.5*DY(IN-1))))
C
      DO 35 I=2,IJ
      A(I)=-0.5*A2
      B(I)=A1
      C(I)=-0.5*A2
C
      D(I)=A3*TB(I,IN)-(ALPHA*(TB(I,IN)-TB(I,IN-1))
     */(DY(IN)*(DY(IN)+0.5*DY(IN-1))))
C
   35 CONTINUE
C
      A(IM)=-A2
      B(IM)=A1
      C(IM)=0.0
C
      D(IM)=A3*TB(IM,IN)-(ALPHA*(TB(IM,IN)-TB(IM,IN-1))
     */(DY(IN)*(DY(IN)+0.5*DY(IN-1))))
C
      CALL TRIDAG(1,IM,A,B,C,D,TPRIME)
      DO 40 I=1,IM
   40 TS(I,IN)=TPRIME(I)
      RETURN
      END
C
C
C
```

```
      SUBROUTINE SNDS(TS,T,DY,DX,DT,ALPHA,IN,IM,TMP,ID,A1,A2,A3)
C
      DIMENSION TS(100,100),T(100,100),DY(100),ID(100)
      DIMENSION A(100),B(100),C(100),D(100),TPRIME(100)
      IF(ID(1)-1) 1,2,2
    2 CALL SOURCE(A(1),B(1),C(1),D(1),TMP)
      GO TO 3
    1 A(1)=0.0
      B(1)=A3+ALPHA/(DY(1)*(DY(1)+0.5*DY(2)))
      C(1)=-ALPHA/(DY(1)*(DY(1)+0.5*DY(2)))
C
      D(1)=A3*TS(1,1)+A2*(TS(2,1)-TS(1,1))
    3 CONTINUE
C
      IJ=IM-1
      IK=IN-1
      DO 10 J=2,IK
C
      A(J)=-2.0*ALPHA/(DY(J)*(DY(J)+DY(J-1)))
C
      B(J)=A3+(2.0*ALPHA/(DY(J)*(DY(J)+DY(J+1))))
     *+(2.0*ALPHA/(DY(J)*(DY(J)+DY(J-1))))
C
      C(J)=-2.0*ALPHA/(DY(J)*(DY(J)+DY(J+1)))
C
      D(J)=A3*TS(1,J)+A2*(TS(2,J)-TS(1,J))
   10 CONTINUE
C
      A(IN)=-ALPHA/(DY(IN)*(DY(IN)+0.5*DY(IN-1)))
C
      B(IN)=A3+ALPHA/(DY(IN)*(DY(IN)+0.5*DY(IN-1)))
C
      C(IN)=0.0
C
      D(IN)=A3*TS(1,IN)+A2*(TS(2,IN)-TS(1,IN))
C
C
C
      CALL TRIDAG(1,IN,A,B,C,D,TPRIME)
C
      DO 15 J=1,IN
   15 T(1,J)=TPRIME(J)
C
      DO 20 I=2,IJ
      IF(ID(I)-1) 4,5,5
    5 CALL SOURCE(A(1),B(1),C(1),D(1),TMP)
      GO TO 6
C
    4 A(1)=0.0
      B(1)=A3+ALPHA/(DY(1)*(DY(1)+0.5*DY(2)))
C
      C(1)=-ALPHA/(DY(1)*(DY(1)+0.5*DY(2)))
C
      D(1)=A3*TS(I,1)+0.5*A2*(TS(I+1,1)+TS(I-1,1)-
     *2.0*TS(I,1))
    6 CONTINUE
C
      DO 30 J=2,IK
C
      A(J)=-2.0*ALPHA/(DY(J)*(DY(J)+DY(J-1)))
```

```
C
      B(J)=A3+2.0*ALPHA/(DY(J)*(DY(J)+DY(J+1)))+
     *2.0*ALPHA/(DY(J)*(DY(J)+DY(J-1)))
C
      C(J)=-2.0*ALPHA/(DY(J)*(DY(J)+DY(J+1)))
C
      D(J)=A3*TS(I,J)+(0.5*A2*((TS(I+1,J)+TS(I-1,J))-
     *2.0*TS(I,J)))
C
   30 CONTINUE
C
      A(IN)=-ALPHA/(DY(IN)*(DY(IN)+0.5*DY(IN-1)))
C
      B(IN)=A3-A(IN)
C
      C(IN)=0.0
C
      D(IN)=A3*TS(I,IN)+0.5*A2*(TS(I+1,IN)+TS(I-1,IN)-
     *2.0*TS(I,IN))
C
      CALL TRIDAG(1,IN,A,B,C,D,TPRIME)
C
      DO 40 J=1,IN
      T(I,J)=TPRIME(J)
   40 CONTINUE
   20 CONTINUE
C
      IF(ID(IM)-1) 7,8,8
    8 CALL SOURCE(A(1),B(1),C(1),D(1),TMP)
      GO TO 9
C
    7 A(1)=0.0
      B(1)=A3+ALPHA/(DY(1)*(DY(1)+0.5*DY(2)))
C
      C(1)=-ALPHA/(DY(1)*(DY(1)+0.5*DY(2)))
C
      D(1)=A3*TS(IM,1)-A2*(TS(IM,1)-TS(IM-1,1))
    9 CONTINUE
C
      DO 50 J=2,IK
C
      A(J)=-2.0*ALPHA/(DY(J)*(DY(J)+DY(J-1)))
C
      C(J)=-2.0*ALPHA/(DY(J)*(DY(J)+DY(J+1)))
C
      B(J)=A3-A(J)-C(J)
C
      D(J)=A3*TS(IM,J)-A2*(TS(IM,J)-TS(IM-1,J))
   50 CONTINUE
C
      A(IN)=-ALPHA/(DY(IN)*(DY(IN)+0.5*DY(IN-1)))
C
      B(IN)=A3-A(IN)
      C(IN)=0.0
C
      D(IN)=A3*TS(IM,IN)-A2*(TS(IM,IN)-TS(IM-1,IN))
C
      CALL TRIDAG(1,IN,A,B,C,D,TPRIME)
C
      DO 60 J=1,IN
```

```
   60 T(IM,J)=TPRIME(J)
      RETURN
      END
C
C
C
      SUBROUTINE SOURCE(A,B,C,D,T)
C
      A=0.0
      B=1.0
      C=0.0
      D=T
      RETURN
      END
C
C
C
      SUBROUTINE PRINT(T,TIME,IN,IM,IP,PRNT,PRNTO,TLAST,ID)
C
C
C
      DIMENSION T(100,100),ID(100)
      IP=0
      IF(TIME.GT.TLAST) GO TO 1
C
      IF(TIME.LT.PRNT) GO TO 2
C
C      WRITE(8,100) TIME
C 100 FORMAT(1H ,21X,'TIME=',F10.1)
C
      DO 10 I=1,IM
      K=I
      IF(ID(K)-1) 10,20,20
   20 WRITE(8,200) (T(I,J),J=1,8),K
  200 FORMAT(8(F6.1,1X),I3)
   10 CONTINUE
      PRNT=PRNT+PRNTO
      GO TO 2
    1 IP=1
    2 RETURN
      END
C
C
C
C
C     SUBROUTINE "TRIDAG" FROM 'APPLIED NUMERICAL METHODS' BY
C     CARNAHAN, LUTHER AND WILKES
C
C
C     SUBROUTINE FOR SOLVING A SYSTEM OF LINEAR SIMULTANEOUS
C     EQUATIONS HAVING A TRIDIAGONAL COEFFICIENT MATRIX.
C     THE EQUATIONS ARE NUMBERED IF THROUGH L AND THEIR
C     SUB-DIAGONAL, DIAGONAL AND SUPER-DIAGONAL COEFFICIENTS
C     ARE STORED IN THE ARRAYS A, B AND C. THE COMPUTED
C     SOLUTION VECTOR IS STORED IN THE ARRAY V.
C
C
C
C
     SUBROUTINE TRIDAG(IF,L,A,B,C,D,V)
```

```
      DIMENSION A(100),B(100),C(100),D(100),V(100)
      DIMENSION BETA(101),GAMMA(101)
C
C
C
C#### COMPUTE INTERMEDIATE ARRAYS BETA AND GAMMA...
C
      BETA(IF)=B(IF)
      GAMMA(IF)=D(IF)/BETA(IF)
      IFP1=IF+1
      DO 10 I=IFP1,L
      BETA(I)=B(I)-A(I)*C(I-1)/BETA(I-1)
      GAMMA(I)=(D(I)-A(I)*GAMMA(I-1))/BETA(I)
   10 CONTINUE
C
C#### COMPUTE FINAL SOLUTION VECTOR V...
C
      V(L)=GAMMA(L)
      LAST=L-IF
      DO 20 K=1,LAST
      I=L-K
      V(I)=GAMMA(I)-C(I)*V(I+1)/BETA(I)
   20 CONTINUE
      RETURN
      END
C
C
C
C
C
C     HEAT BALANCE USED TO CALCULATE THE NEW BOUNDARY TEMPERATURE
C     AT EVERY TIME STEP
C
      SUBROUTINE HEAT(XI,VO,AK,CP,RO,DX,DPH,TH,T,TMP,ID,G,F,IM,IN,
     *TBO,DY,DT,V,TIME,SE,SWG,AL,FR,CPW,DELT,ROW,HEB,BF)
      DIMENSION ID(100),T(100,100),DY(100)
      Q1=0.0
      NO=IFIX(V*TIME/DX+0.51)+1
      NS=IFIX((DPH+V*TIME)/DX+0.49)+1
      NN=NO-1
      IF(NO-1) 1,1,2
    2 DO 15 K=1,NN
      ID(K)=0
   15 CONTINUE
    1 DO 25 M=NO,NS
      ID(M)=1
   25 CONTINUE
      NNS=NS+1
      DO 35 J=NNS,IM
      ID(J)=0
   35 CONTINUE
      BETA=((SE/SWG)/(1.-(SE/SWG)))
      DO 10 I=1,IM
      IF(ID(I)-1) 10,20,20
   20 Q1=Q1-((AK*DX*TH)*((4*T(I,2)-T(I,3)-3*TMP)/
     *(DY(1)+DY(2))))
   10 CONTINUE
      WRITE(6,990) Q1,BETA
  990 FORMAT(1H ,'HEAT INPUT=',1X,F15.2,/,F8.5,1X,/)
      CE=CP*RO*DPH*TH*G
```

```
      TS=TMP-(((Q1*DT*HEB)/(CE))-((XI*VO*F*DT*.228)/(CE))
     *+((AL*(1./BETA)*V*DT)/(CP*DPH)))
      TMP=TS
      WRITE(6,999) TMP,V
  999 FORMAT(1H ,'TMP=',1X,F7.2,/,F7.2)
      RETURN
      END
C
C
C
      SUBROUTINE HEAT1(AK,DX,TH,T,DY,ID,Q1,IM,DPH,DT,IN,TBO,TMP)
      DIMENSION ID(100),T(100,100),DY(100)
      DO 4 I=1,IM
      DO 6 J=1,IN
      T(I,J)=TBO
    6 CONTINUE
    4 CONTINUE
      Q1=0.0
      TIME=DT
      NO=IFIX(0.05*TIME/DX+0.51)+1
      NS=IFIX((DPH+0.05*TIME)/DX+0.49)+1
      NN=NO-1
      IF(NO-1) 1,1,2
    2 DO 10 K=1,NN
      ID(K)=0
   10 CONTINUE
    1 DO 20 M=NO,NS
      ID(M)=1
   20 CONTINUE
      NNS=NS+1
      DO 30 J=NNS,IM
      ID(J)=0
   30 CONTINUE
      DO 5 I=1,IM
      IF(ID(I)-1) 5,50,50
   50 Q1=Q1-((AK*DX*TH)*((4*T(I,2)-T(I,3)-3*TMP)/
     *(DY(1)+DY(2))))
    5 CONTINUE
      WRITE(6,897) Q1
  897 FORMAT(1H ,1X,'HEAT INPUT=',F15.1)
      RETURN
      END
C
C      THERMAL STRESS CALCULATION PERFORMED FOR EACH NODAL
C      TEMPERATURE
C
      SUBROUTINE STRESS(T,TT,TTT,IT,IM,IN,ALFA,H)
      DIMENSION T(500,20),TT(500),TTT(500)
      DO 10 I=1,IT
      READ(5,100) (T(IT,IN),IN=1,8)
  100 FORMAT(8(F6.1,1X))
   10 CONTINUE
C CALCULATION OF E(YOUNG'S MODULUS) AS A FUNCTION OF TEMPERATURE
C
      DO 11 L=1,IM
      DO 12 J=1,8
      DO 14 I=1,IT
      TT(I)=T(I,J)
      TTT(I)=TT(I)*L
      IF(TT(I) .LT. 1000.) GO TO 1
```

```
      E=0.000012
    1 IF(TT(I) .GE. 1000. .AND. TT(I) .LE. 1400.) GO TO 2
      E=(2000.-(1.875*(TT(I)-1000.)*100000.))
    2 IF(TT(I) .GE. 1400. .AND. TT(I) .LE. 1475.) GO TO 3
      E=((1250.*(1475.-TT(I))/75.)*10000.)
    3 IF(TT(I) .GT. 1475.) GO TO 14
      E=0.0
      AREA1=QINT4P(I,TT(I),465,1,465)
      AREA2=QINT4P(I,TTT(I),465,1,465)
      SIGMA=(-ALFA*E*TT(I)+((0.5*H)*(ALFA*E*AREA1))
     *+(((1.5*L)/(H**3.))*(ALFA*E*AREA2)))
      WRITE(7,200) SIGMA
  200 FORMAT(1H ,2X,'THERMAL STRESS=',F8.3)
   14 CONTINUE
   12 CONTINUE
   11 CONTINUE
      RETURN
      END
C
C
C
C
C
C                LIST OF SYMBOLS USED IN THE MODEL
C
C
C
C
C
C          TMP = Melting point temperature(Deg. C)
C
C          TBO = Parent metal initial temperature(Deg. C)
C
C          DT = Time step(s)
C
C          CP = Specific heat of steel(cal/g.deg.C)
C
C          RO = Density of steel(g/cm**3)
C
C          AK = Thermal conductivity of steel(cal/cm.s.deg. C)
C
C          DX = Space increment in X-direction(cm)
C
C          DY = Space increment in Y-direction(cm)
C
C          V  = Welding velocity(cm/s)
C
C          DPH = Slag + liquid metal depth(cm)
C
C          PRNT = Print cycle(s)
C
C          TLAST = End of calculation(s)
C
C          IM = # of divisions in the X-direction
C
C          IN = # of divisions in the Y-direction
C
C          T = Temperature(deg. C)
C
C          XI = Current(A)
```

```
C
C          VO = Voltage(V)
C
C          TH = Thickness(cm)
C
C          G = Weld gap(cm)
C
C          F = Efficiency factor
C
C          SE = Electrode area(cm**2)
C
C          SWG = Weld gap area(cm**2)
C
C          AL = Latent heat(cal/g)
C
C          FR = Fill ratio
C
C          ALFA = Coefficient of expansion(/deg. C)
C
C          H = Weld height(cm)
C
C          ID = Heat source contact index
```

APPENDIX C - EFFICIENCY FACTOR AND HEAT SINK CALCULATIONS

Paton[35] reports that about 58.6% of the available heat goes into the blocks when Electroslag Welding(wire electrode). Due to the different thermal characteristics already discussed, for Electroslag Joining that number would not apply. Therefore, new calculations had to be performed based on some measurements:

The cooling shoe water flow rate was measured and found to be 3698 cm^3/s. The electrode melt rate can be calculated as follows:

Melt Rate = Electrode Feed Rate x Area x Density

The electrode feed rate can be ascertained using the following expression given by Frost et al.[41]:

$$E\ F\ R = \frac{1 - FR}{FR} \times V$$

where: E F R = electrode feed rate
F R = fill ratio(electrode area/weld area)
V = welding velocity

For the material dimensions used in most experiments

$$\frac{1-FR}{FR} = 1.6735$$

For an experimental welding velocity of 0.023 cm/s, the EFR was found to be :

E F R = 1.6735 x 0.023 = 0.0385 cm/s

Therefore,

Melt Rate = 0.0385cm/s x 57.912cm^2 x 7.86g/cm^3 = 17.52 g/s

If approximately 400 KWH are needed to melt 1000 kg or 1x10^6 g of steel, then the power for melting would be:

$$P = \frac{17.52\ g/s \times 400\ KWH \times 3600\ s}{1 \times 10^6\ g} = 25.23\ KW$$

The heat flux per mould would then be:

$$H_W = \text{Flow rate} \times Cp_W \times \Delta T \times \rho_W \times \frac{4.1868}{1000} = 85.16 \text{ KW}$$

Therefore,

$$H_M = \frac{25.23}{33 \times 5000 \times .95} = 16.1\%$$

$$H_W = \frac{85.16}{156.75} = 54.3\%$$

$$H_R = \sim 1\ \%$$

$$H_{block} = 100 - \Sigma(H_M + H_W + H_R)$$

$$H_{block} \sim 15\%$$

And, therefore, only about 15 % of the available energy flows through the blocks and is accumulated there. This is the factor used in the model when calculating the heat flow.

****

THE BLOCK AS A HEAT SINK

The amount of heat lost through the block cold face is very small when compared with the heat available from the electrode that is entering the block via the opposite face. In order to see how that is effected a plot of temperature versus distance from the hot face has been generated and illustrated in Fig. 26 The point at which the temperature drops to room temperature has been found to be 61 cm away from the hot face.(Approximately 2 feet)

APPENDIX D - RESIDUAL STRESS EVALUATION

$$\sigma_1 = \frac{(A + B\cos 2\beta)\varepsilon a - (A - B\cos 2\beta)\varepsilon c}{4AB\cos 2\beta}$$

$$\sigma_2 = \frac{(A + B\cos 2\beta)\varepsilon c - (A - B\cos 2\beta)\varepsilon a}{4AB\cos 2\beta}$$

$$\tan 2\beta = \frac{\varepsilon a - 2\varepsilon b + \varepsilon c}{\varepsilon a - \varepsilon c}$$

Position 1 - Parent metal

Depth = 120 thou

$\varepsilon a = -35\mu\varepsilon$ $\varepsilon b = -62\mu\varepsilon$ $\varepsilon c = -143\mu\varepsilon$

$r_1 = \frac{0.200}{0.078} = 2.55$ $4A = -1.35 \times 10^{-8}$

$4B = -3.55 \times 10^{-8}$ (After Redner[46])

Therefore, $A = -3.375 \times 10^{-9}$ and $B = -8.868 \times 10^{-9}$

$\sigma_1 = +9781$ psi

$\sigma_2 = +16589$ psi

Position 2 - Heat affected zone

Depth = 120 thou

$\varepsilon a = +67\mu\varepsilon$ $\varepsilon b = +51\mu\varepsilon$ $\varepsilon c = -225\mu\varepsilon$

$r_2 = \frac{0.2045}{0.071} = 2.87$ $4A = -1.1142 \times 10^{-8}$

$4B = -2.9920 \times 10^{-8}$

Therefore, $A = -2,7855 \times 10^{-9}$ and $B = -7.48 \times 10^{-9}$

$\sigma_1 = +1113$ psi

$\sigma_2 = +27248$ psi

Position 3 - Weld metal

Depth = 120 thou

$\varepsilon a = -152\mu\varepsilon$ $\varepsilon b = -157\mu\varepsilon$ $\varepsilon c = -107\mu\varepsilon$

$r_3 = \frac{0.1885}{0.067} = 2.8$ $4A = -1.1142 \times 10^{-8}$

$4B = -3.0 \times 10^{-8}$

Therefore, $A = -2.7854 \times 10^{-9}$ and $B = -7.5 \times 10^{-9}$

$\sigma_1 = +25615$ psi

$\sigma_2 = +20877$ psi

The residual stress measurement was carried out using the Blind Hole Drilling technique[45] which is a semi-destructive method whereby a small hole, 3.175 mm(1/8") in diameter is drilled to a depth approximately equal to its diameter. The relaxed strains are then measured around the hole.

σ_2 is the longitudinal stress remaining in the welded assembly and σ_1 is at a 90 degree angle to σ_2. They were measured in the parent material, heat affected zone and weld metal.